2013-01-01

Modeling Visibility In The El Paso Del Norte (PdN) Region

Richard Medina Calderon
University of Texas at El Paso, rmedina9@miners.utep.edu

MODELING VISIBILITY IN THE EL PASO DEL NORTE (PDN) REGION

RICHARD MEDINA CALDERON

Computational Sciences Program

APPROVED:

Rosa Fitzgerald, Ph.D., Chair

Marian Manciu, Ph.D.

Rodrigo Romero, Ph.D.

Benjamin C. Flores, Ph.D.
Dean of the Graduate School

Dedication

To my beloved parents Dolores and Bartolo, to my brother Walter, my sisters Teresa, Maria, and Lith, and all their beautiful children, Elvis, Alessandro, Alexa, and Jesus. And finally, special thanks to my wife Carol for her support and availability during all this time . . .

MODELING VISIBILITY IN THE EL PASO DEL NORTE (PDN) REGION

by

RICHARD MEDINA CALDERON, MSc

THESIS

Presented to the Faculty of the Graduate School of

The University of Texas at El Paso

in Partial Fulfillment

of the Requirements

for the Degree of

MASTER OF SCIENCE

Department of Computational Sciences

THE UNIVERSITY OF TEXAS AT EL PASO

May 2013

Acknowledgements

First and foremost to my advisor Rosa Fitzgerald, for all the dedication she put in this work, and for her patience, wise guidance and endless encouragement throughout all this months.

A special thanks to my committee members, Dr. Marian Manciu for being always available to discuss ideas, to Dr. Rodrigo Romero for helping me to analyze data through scientific visualization and also for being part of this committee.

I would also like to thank to my friends at the University of Texas at El Paso, especially to all the people from the laboratory of Atmospheric Physics and from the Computational Sciences program.

Finally, I would like to extend special thanks to Dr. Dave Dubois and the New Mexico Health Agency, for the financial support that made the completion of this work possible.

Abstract

Poor visibility is a subject of growing public concern throughout the U.S, and an active area of research. Its societal impacts on air quality, aviation transport and traffic are significant. Aerosols play a fundamental role in the attenuation of solar radiation, and also affect visibility. The scattering and extinction coefficients of aerosol particles in the Paso del Norte Region have been calculated using the T- matrix model in conjunction with a laser particle counter. Inter-comparison of the model's results of the scattering and absorption coefficients against the corresponding data from a Photoacustic extinctiometer instrument (which measures in-situ absorption and scattering coefficients of aerosol particles) shows excellent agreement. In addition, the volume-weighted method is used to determine the composite index of refraction which is representative of the aerosols for the Paso del Norte Region to obtain information of the type of aerosol particles present in the Region. The Single Scattering Albedo has also been retrieved using this methodology to obtain further insight into the type of aerosols present on a given day. Finally, the Koschmieder equation has been used to calculate the visual range or visibility, and was correlated with the PM2.5 and PM10 particle concentration present in the Region. Our methodology will allow a better understanding of the size and type of aerosol particles that are most detrimental to the visibility for the Paso Del Norte Region.

Table of Contents

List of Tables

List of Figures

Chapter 1. Introduction

The word aerosol [5] denotes an aerial colloid, a suspensoid with air as the medium with radius between $0.5 - 10^{-3}\mu m$ to 20 μm approximately. They arise from emissions of particles and from the conversion of certain gases to particles in the atmosphere [6]. The optical properties of atmospheric aerosols are determined by chemical composition, concentration, size, shape, and internal structure. An important dimensionless parameter for aerosol particles is the ratio a/λ, where λ is the wavelength of incident light and a is the characteristic size of a particle (e.g., the radius of a droplet, or the side of a cubic crystal). The number concentration N represents the number of particles per cubic centimeter and is also an important quantity when studying aerosols. For example the number concentration of sea salt particles in the open ocean is usually around 250 cm^{-3} (250 particles per cubic centimeter). In this case, the value of N is dominated by small particles with typical sizes around $0.3\mu m$, and the particle size distribution (PSD), which is expressed as a function of radius $f(a)$) and modeled using the lognormal law:

$$f(a) = \frac{1}{\sqrt{2\pi}\sigma a}\exp\{-\frac{\ln^2(a/a_0)}{2\sigma^2}\} \quad (1)$$

where a is the radius of a spherical homogeneous particle, $a_0 = 0.3\ \mu m$ is the effective radius (which is an area weighted mean radius of the aerosol particle), and σ is the standar deviation corresponding to this distribution. The lognormal distribution often provides a good fit and is regularly used in atmospheric applications [6].

The effective radius a_{eff} and effective variance v_{eff} are important quantities in aerosol optics. They are defined as follows:

$$a_{\text{eff}} = \frac{\int_0^\infty a^3 f(a)da}{\int_0^\infty a^2 f(a)da}$$

$$v_{\text{eff}} = \frac{\int_0^\infty (a - a_{\text{eff}})^2 \, a^2 f(a) da}{a_{\text{eff}}^2 \int_0^\infty a^2 f(a) da} \tag{2}$$

or, in this case for the lognormal particle size distribution the following relations apply

$$a_{\text{eff}} = a_0 \exp(2.5\sigma^2)$$

$$v_{\text{eff}} = \exp(\sigma^2) - 1 \tag{3}$$

An important property of aerosols is the *optical depth*, which is a measure of the transparency (dimensionless), or the quantity of light radiation removed from a beam by scattering or absorption.

$$\tau(z, \nu) = -\int_{z_1}^{z_2} B_{ext}(z', \nu) \, dz' \tag{4}$$

The negative sign is used because we shall adopt the convention that z and τ run in opposite directions. The value of $\tau_\nu(z)$ gives the integrated absorption of radiation along the z-direction in the segment $(z_2 - z_1)$. The term B_{ext} is the extinction coefficient which is defined as the attenuation of radiation after passing through a medium, ν is the wavelength frequency and z is the vertical coordinate. The interaction of optical waves with aerosol particles depends on the relative complex refraction index $n = m - ik$, where k represents the ability of the particle to absorb electromagnetic energy. The refractive index of water, for example is approximately 1.33 in the visible and its complex refractive index is 1.000×10^{-9} indicating that the water is very low absorptive of light radiation and it can be neglected in the visible and also in the ultraviolet regime where $\text{k} = 1.1000 \times 10^{-7}$.

Aerosols can also be classified by their origin, for example due to gas-to-particle conversion which are composed of sulfates and nitrates, biological aerosols which are present in form of pollen, fungal spores, bacteria, viruses, etc., or smoke aerosols produced by different types of fires. In the last case, it is important to highlight that _res produce around 5 million tons of particulate matter per year [7], but still this is a small number compared to the load of other aerosols, however it has important effects in reducing visibility, causing biosphere diseases and over global climate.

Table 1 shows us the refractive values of some aerosols for some wavelengths from ultraviolet to infrared. As it was mentioned, values of m give us both the scattering index of the particle and k the absorption index of refraction of the particle.

Table 1: The refractive index $n = m - ik$ of oceanic, water-insoluble (mainly, dust), water-soluble (sulfates, nitrates, etc.), and soot aerosol, respectively (courtesy of Kokhanovsky, A. [1])

λ, **nm**	n	k	n	k	n	k	n	k
300	1.40	5.8×10^{-7}	1.53	8.0×10^{-3}	1.53	8.0×10^{-3}	1.74	0.47
400	1.39	9.9×10^{-9}	1.53	8.0×10^{-3}	1.53	5.0×10^{-3}	1.75	0.46
550	1.38	4.3×10^{-9}	1.53	8.0×10^{-3}	1.53	6.0×10^{-3}	1.75	0.44
694	1.38	5.0×10^{-8}	1.53	8.0×10^{-3}	1.53	7.0×10^{-3}	1.75	0.43
860	1.37	1.1×10^{-6}	1.52	8.0×10^{-3}	1.52	1.2×10^{-2}	1.75	0.43
1060	1.37	6.0×10^{-5}	1.52	8.0×10^{-3}	1.52	1.7×10^{-2}	1.75	0.44
1300	1.37	1.4×10^{-4}	1.46	8.0×10^{-3}	1.51	2.0×10^{-2}	1.76	0.45
1800	1.35	3.1×10^{-4}	1.33	8.0×10^{-3}	1.46	1.7×10^{-2}	1.79	0.48
2000	1.35	1.1×10^{-3}	1.26	8.0×10^{-3}	1.42	8.0×10^{-3}	1.80	0.49
2500	1.31	2.4×10^{-3}	1.18	9.0×10^{-3}	1.42	1.2×10^{-2}	1.83	0.51

Most of the concentrations of aerosol particles are in the first 2000 m (or 2 km) of the troposphere, inside a region that is known as the Boundary Layer. The boundary layer is the region from the surface to about 0.5-3.0 km altitude and its height changes during the day. Figure 1 shows the concentration of aerosol particles expressed by its optical depth for the first 10 km in the city of El Paso for a light wavelength of 500 nm (1 nm = 10^{-9}m). This figure is a re-creation of the values of optical thickness vertical profile of Elterman L., at 500 nm [8], and weighted with local values for the surface of

El Paso. It clearly shows that most of the concentrations of aerosols are in the first 2 km of the troposphere, inside the boundary layer.

In the El Paso del Norte topography, most of the aerosols correspond to mineral dust and sand which originate from the land surface, and with some contributions of anthropogenic sources. Mineral dust and sand are the primary elements that reduce visibility and also affect the health of the residents in the region, especially in high-wind events where the concentration of particles can reduce the visibility to 5%.

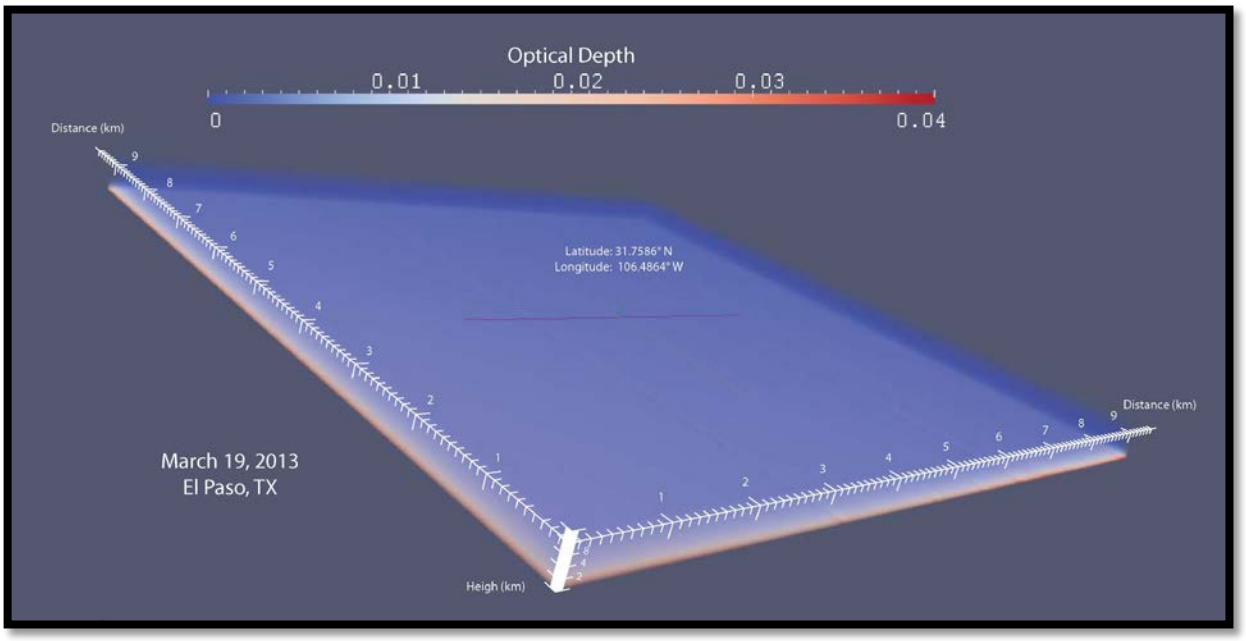

Figure 1: Aerosol vertical distribution at 500 nm, for El Paso, TX.

1.1 OPTICAL PROPERTIES OF ATMOSPHERIC AEROSOLS

Light is scattered by aerosol particles suspended in the air. Processes of light scattering mostly dominate over processes of absorption in the visible region. The reduction in the intensity of a direct beam during its propagation through an aerosol medium is determined simultaneously by absorption and scattering

processes. Emission, which is negligible at optical wavelengths, is not considered in light scattering processes.

All solar radiation with wavelength below 0.28 μm is absorbed by the Earth's atmosphere, above the troposphere. The troposphere is a region that starts at the surface and extends to between 9 km at the poles and 17 km at the equator, although this extension can vary with the weather.

Above the troposphere there are several layers where a different phenomenon occurs. Figure 2 depicts what is called the lower atmosphere and its layers along with the distribution of the temperatures and pressures with the altitude.

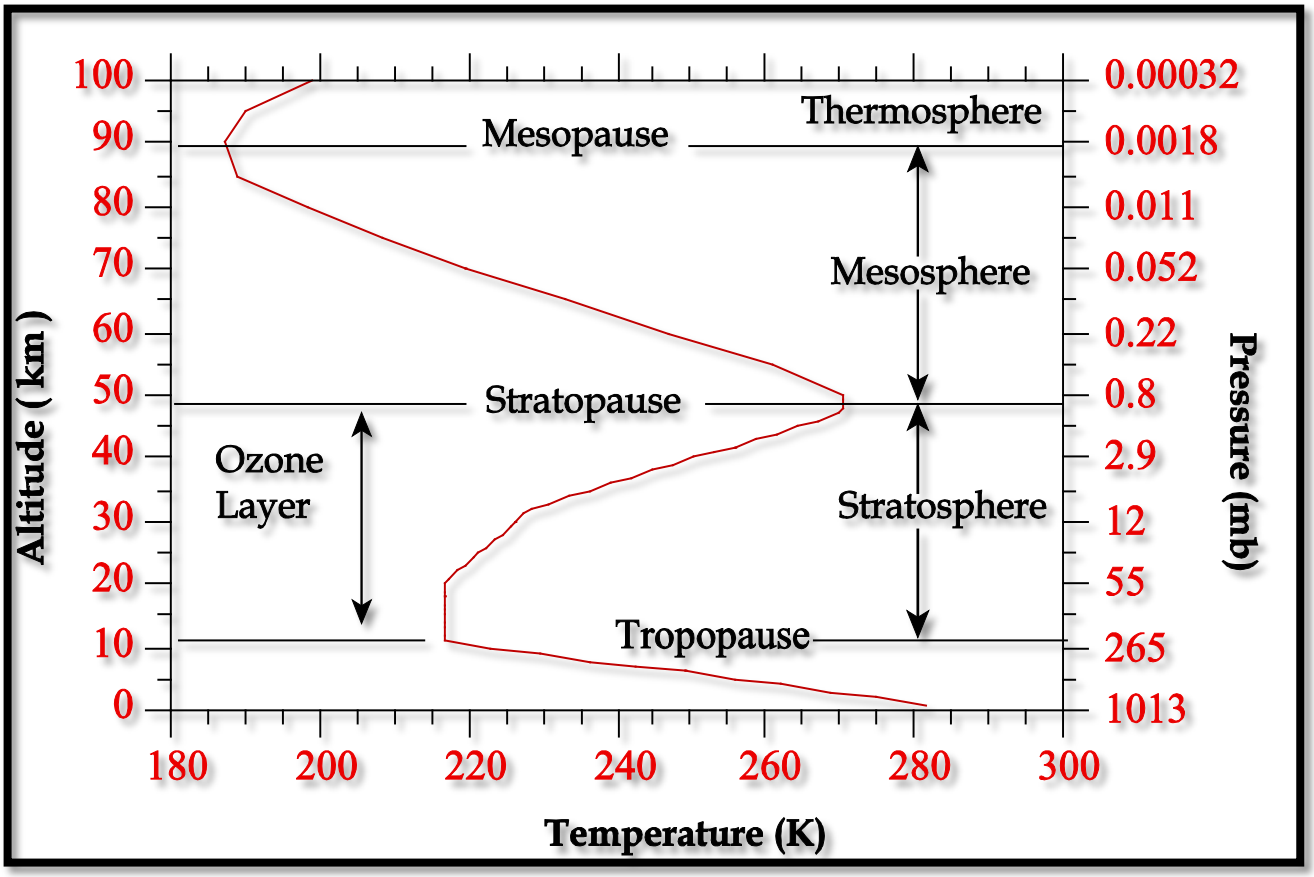

Figure 2: Layers of the Earth's lower atmosphere, and the structure of the temperature and pressure with the altitude. Courtesy of Jacobson M. Z. [3].

Gas absorption is important only in the thermosphere (320-380 km), mesosphere (50-85 km approximately) and stratosphere (12-51 km, approximately), where N_2 and O_2 together prevent those wavelengths less than 0.245 μm reaching the troposphere [3].

In the troposphere only NO_2 affects more visibility, especially for wavelengths less than 0.50 μm and moderately for wavelengths of 0.5-0.6μm. At wavelengths less than 0.32 μm however, O_3 has a larger effect than NO_2 on visibility. On the other side, the only process of gas scattering by gas in the atmosphere is Rayleigh scattering which is produced by N2 and O2 mainly [9].

In summary, gases scatter short wavelength much more effectively than they do long wavelength and also their mixing ratios are too low in comparison with the effect of scattering and absorption by particles. It is for this reason that the study of visibility is concentrated only on aerosol particles in the troposphere.

In the case of absorption, the imaginary part k, of the refractive index is an important parameter because the greater the absorption of a particle, the lesser the scattering, since absorption hinders scattering. Small particles ($r_i \ll \lambda$) are relatively inefficient absorbers of radiation. The strongest absorptive particle in the visible and ultraviolet spectrum region is black carbon, which is the main component of soot. Others are Fe_2O_3, Al_2O_3, and certain organic compounds [3].

The description of range and regimen of particles and wavelengths is important when we study the effects of extinction of solar radiation due to the interaction with aerosol particles. When a particle diameter is much smaller than the wavelength of light ($d_i < 0.03\lambda$), it is said that the particles are in the Rayleigh regime. For diameter particles in $0.03\lambda < d_i < 32\lambda$, the particles are in the Mie region, and the absorption and scattering are approximated with Mie's solution to Maxwell equations (or with the Tmatrix approximation, which has a wider application for different shapes of particles than Mie's approximation which only deals with spherical shapes). Finally, for diameters of $d_i > 32\lambda$, the particles are in the Geometric regime.

1.2 EXTINCTION, SCATTERING, AND ABSORPTION BY AN ARBITRARY FINITE PARTICLE

When an incident electromagnetic beam impinges on a small particle, several effects can be caused. When the energy is absorbed into the particle, the process is called absorption and the energy is converted into heat. If the energy is scattered into any direction, this process is called scattering. As a result, the energy is reduced by an amount equal to the sum of the absorbed and scattered energy and it is called extinction. Extinction (or attenuation), is the effect that produces a diminishing in intensity of radiation through a medium due to either absorption or scattering, or both together. The spectral aerosol extinction coefficient is defined as

$$B_{\text{ext}} = NC_{\text{ext}} \tag{5}$$

also, the equivalent spectral aerosol scattering coefficient is defined by

$$\mathrm{B_{sca}} = \mathrm{NC_{sca}} \tag{6}$$

and the equivalent spectral aerosol absorption coefficient

$$B_{\text{abs}} = NC_{\text{abs}} \tag{7}$$

are important physical quantities that will allow us to calculate levels of visibility in this work. In equations (5), (6), and (7), N is the number of particles in a unit volume and

$$C_{\text{ext}} = C_{\text{abs}} + C_{\text{sca}} \tag{8}$$

where C_{ext}, C_{abs}, and C_{sca} are the extinction, absorption, and scattering cross section respectively.

The extinction, scattering and absorption cross sections are characteristics of the scattering object. The product of the scattering cross section C_{sca} and the incident monochromatic energy flux gives the total monochromatic power removed from the incident wave as a result of scattering of the incident radiation in all directions. Analogously, the product of the absorption cross section C_{abs} and the incident monochromatic energy flux gives the total monochromatic power removed from the incident wave as a result of absorption of light by the object [10]. In consequence, the extinction cross section C_{ext} is the sum of the scattering and absorption cross sections and, when multiplied by the incident

monochromatic energy flux, the total monochromatic power removed from the incident light by the combined effect of scattering and absorption is obtained.

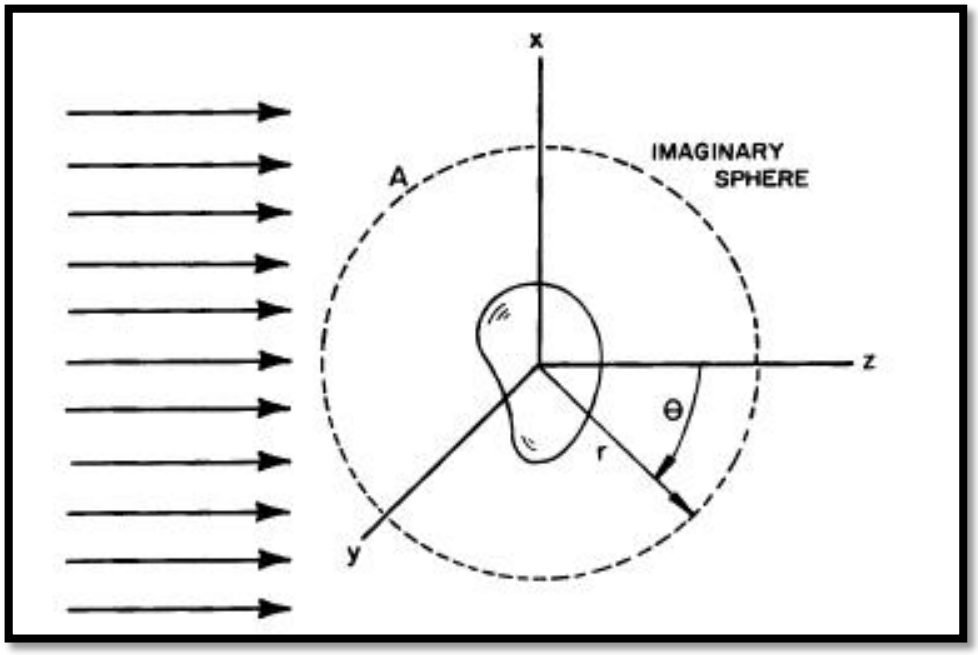

Figure 3: Extinction by a single particle. Courtesy of Bohren, C. F. [4].

To determine the total optical cross sections, an imaginary non-absorbing medium as a sphere of radius r and area S is constructed around the particle as is shown in figure 3. The net rate at which electromagnetic energy crosses the surface S of this sphere is always non-negative and is equal to the power absorbed by the particle:

$$W_{\text{abs}} = -\int_S \langle \boldsymbol{S}(\boldsymbol{r}) \rangle \, \hat{\boldsymbol{r}} \, dS = -\mathrm{r}^2 \int_{4\pi} \langle \boldsymbol{S}(\boldsymbol{r}) \rangle \, \hat{\boldsymbol{r}} \, d\hat{\boldsymbol{r}} \tag{9}$$

here **S** is the Poynting vector which specifies the magnitude and direction of the rate of transfer of electromagnetic energy at all points of space, namely

$$\mathbf{S} = \mathbf{E} \times \mathbf{H} \tag{10}$$

or for the time averaged Poynting vector for time harmonic fields

$$\langle \mathbf{S} \rangle = \frac{1}{2} \mathbf{Re}\{\mathbf{E_c} \times \mathbf{H_c^*}\} \tag{11}$$

where the sub index c denotes complex vector and $\mathbf{H_c}$ denotes the complex conjugate of the magnetic field. Now, W_{abs} can be written as a combination of three terms

$$W_{\text{abs}} = W_{\text{inc}} - W_{\text{sca}} + W_{\text{ext}} \tag{12}$$

where

$$W_{\text{inc}} = -\text{r}^2 \int_{4\pi} \langle \boldsymbol{S}_{\text{inc}}(\boldsymbol{r}) \rangle \, \hat{\boldsymbol{r}} \, d\hat{\boldsymbol{r}} \tag{13a}$$

$$W_{\text{sca}} = -\text{r}^2 \int_{4\pi} \langle \boldsymbol{S}_{\text{sca}}(\boldsymbol{r}) \rangle \, \hat{\boldsymbol{r}} \, d\hat{\boldsymbol{r}} \tag{13b}$$

$$W_{\text{ext}} = -\text{r}^2 \int_{4\pi} \langle \boldsymbol{S}_{\text{ext}}(\boldsymbol{r}) \rangle \, \hat{\boldsymbol{r}} \, d\hat{\boldsymbol{r}} \tag{13c}$$

W_{inc} vanishes because the surrounding medium is non-absorbing and $\mathbf{S}_{\text{inc}}(\boldsymbol{r})$ is a constant vector independent of *r*, whereas W_{sca} is the rate at which the scattered energy crosses the surface S in the outward direction. Therefore, W_{ext} is equal to the sum of the energy scattering rate and the energy absorption rate:

$$W_{\text{abs}} = W_{\text{sca}} + W_{\text{ext}} \tag{14}$$

And now, the W_{ext}, W_{abs}, and W_{sca}, can be related with I_i which is the incident radiance and the respective cross section values

$$W_{\text{ext}} = \frac{W_{\text{ext}}}{I_{\text{inc}}} \tag{15a}$$

$$W_{\text{abs}} = \frac{W_{\text{abs}}}{I_{\text{inc}}} \tag{15b}$$

$$W_{\text{sca}} = \frac{W_{\text{sca}}}{I_{\text{inc}}} \tag{15c}$$

1.2.1 The scattering matrix

The calculation of the electromagnetic fields inside and scattered by a particle due to its interaction with light is an interesting problem treated in many books (see for example [4], [11], and [12]), where the main idea is solving the vector wave equations for **E** and **H**

$$(\nabla^2 + \mathrm{k}^2)\mathbf{E} = 0 \tag{16a}$$

$$(\nabla^2 + \mathrm{k}^2)\mathbf{H} = 0 \tag{16b}$$

where $k^2 = \omega^2\varepsilon\mu$, with μ as the magnetic permeability, which measure the ability of magnetization of a material in response to a magnetic field, and ε is the complex permittivity. The complex permittivity can be expressed as

$$\varepsilon = \varepsilon_0(1 + \chi) + i\frac{\sigma}{\omega} \tag{17}$$

where χ is the electric susceptibility (a measure of how fast a dielectric polarizes in response to an electric field), σ is the electric conductivity of the medium, ε_0 is the permittivity of free space (ε_0= 8.854187× 10^{-12}F/m), which is the material's ability to transmit an electric field, and ω is the angular frequency of the field. The calculated electromagnetic fields allow the determination of the Poynting vector at points outside the particle (see figure 4). By using the equation (11), the Poyinting vector **S** at any point in the medium surrounding the particle can be written as the sum of three terms

$$\mathbf{S} = \frac{1}{2}\mathbf{Re}\{\mathbf{E_2} \times \mathbf{H_2^*}\} = \mathbf{S_{inc}} + \mathbf{S_{sca}} + \mathbf{S_{ext}}$$

$$\mathbf{S_{inc}} = \frac{1}{2}\mathbf{Re}\{\mathbf{E_{inc}} \times \mathbf{H_{inc}^*}\}, \qquad \mathbf{S_{sca}} = \frac{\mathbf{1}}{\mathbf{2}}\mathbf{Re}\{\mathbf{E_{sca}} \times \mathbf{H_{sca}^*}\} \tag{18}$$

$$\mathbf{S_{ext}} = \frac{\mathbf{1}}{\mathbf{2}}\mathbf{Re}\{\mathbf{E_{inc}} \times \mathbf{H_{sca}^*} + \mathbf{E_{sca}} \times \mathbf{H_{inc}^*}\}$$

If the medium is nonabsorbent, $\mathbf{S_{inc}}$ is independent of the position and we may interpret $\mathbf{S_{ext}}$ as the term that arises because of the interaction between the incident and scattered waves. The problem of scattering is in this sense a problem that is more related to the polarization of light (quasi-

monochromatic light), which is nicely represented by a column vector called the Stokes vector [13], with its four elements which are called the Stokes parameter. The theory of light scattering and Stokes parameters was introduced into optics by Sir George Gabriel Stokes in 1852 when he was trying to describe mathematically the nature of polarized light, but his work was not followed immediately until almost one century after when it was "rediscovered" by S. Chandrasekar in the late 1940s when he wrote his monumental paper on radiative transfer [14].

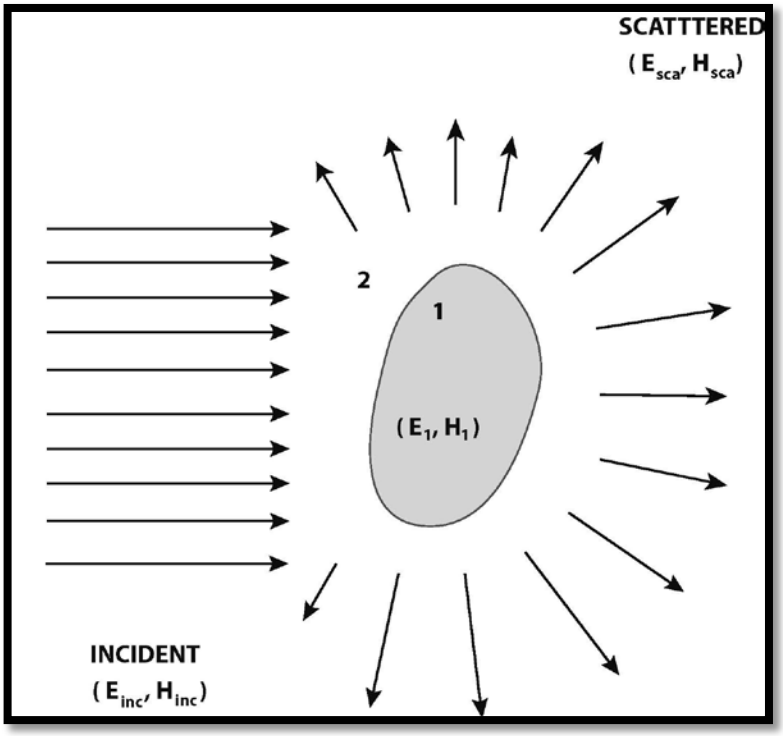

Figure 4: The incident field ($\mathbf{E}_{inc,}\ \mathbf{B}_{inc}$) gives rise to a field ($\mathbf{E}_{1,}\ \mathbf{B}_{1}$) inside the particle and a scattered field ($\mathbf{E}_{sca}$, $\mathbf{B}_{sca}$) in the surrounding medium of the particle labeled as 2. Courtesy of Bohren, F. C. [4].

The Stokes parameter of the light scattered by a particle are

$$I_{\text{sca}} = \frac{k}{2\omega\mu} \quad \langle E_{||\text{sca}} E^*_{||\text{sca}} + E_{\perp\text{sca}} E^*_{\perp\text{sca}} \rangle$$

$$
\begin{aligned}
Q_{\text{sca}} &= \frac{k}{2\omega\mu} \ \langle E_{||\text{sca}} E^*_{||\text{sca}} - E_{\perp\text{sca}} E^*_{\perp\text{sca}} \rangle \\
U_{\text{sca}} &= \frac{k}{2\omega\mu} \ \langle E_{||\text{sca}} E^*_{\perp\text{sca}} + E_{\perp\text{sca}} E^*_{||\text{sca}} \rangle \\
V_{\text{sca}} &= \frac{k}{2\omega\mu} \ \langle E_{||\text{sca}} E^*_{\perp\text{sca}} - E_{\perp\text{sca}} E^*_{||\text{sca}} \rangle
\end{aligned}
\tag{19}
$$

The parameters in equation (19) represent the total intensity of the light (I_{sca}), the amount of linear horizontal or vertical polarization (Q_{sca}), the amount of 45$^{\text{o}}$ or - 45$^{\text{o}}$ degrees polarization (U_{sca}), and the amount of right or left circular polarization (V_{sca}) for scattered light. It turns out that the Poynting vector is directly proportional to the first Stokes parameter *I*.

The relation between incident and scattered Stokes parameters are expressed in the following formula

$$
\begin{bmatrix} I_{\text{sca}} \\ Q_{\text{sca}} \\ U_{\text{sca}} \\ V_{\text{sca}} \end{bmatrix} = \frac{1}{k^2 r^2} \ \begin{bmatrix} S_{11} & S_{12} & S_{13} & S_{14} \\ S_{21} & S_{22} & S_{23} & S_{24} \\ S_{31} & S_{32} & S_{33} & S_{34} \\ S_{41} & S_{42} & S_{43} & S_{44} \end{bmatrix} \begin{bmatrix} I_{\text{inc}} \\ Q_{\text{inc}} \\ U_{\text{inc}} \\ V_{\text{inc}} \end{bmatrix}
\tag{20}
$$

where the 4×4 matrix in equation (20) is the scattering matrix or the Müller matrix and it describes the relation between "incident and "transmitted" Stokes vectors.

The Stokes parameters of the light scattered by a collection of particles are the sum of the Stokes parameters of the light scattered by individual particles. Therefore the scattering matrix for such a collection is merely the sum of individual particle scattering matrices, assuming that the linear dimensions of the volume occupied by the scatterers is small compared with the distance r at which the scattered light is observed [4].

1.3 THE TMATRIX APPROXIMATION

The T-matrix method is a powerful technique for computing light scattering by non-spherical single and compounded particles in random orientation and it is based on numerically solving Maxwell's equations [10]. It was first introduced by Waterman (1965, 1971) as a technique for computing electromagnetic scattering by single, homogeneous, arbitrarily shaped particles based on the Huygens principle ([15], [16], [17], and [18]).

The single scattering of light by a small-volume element dV of n particles randomly oriented, and rotationally symmetric, is completely described by the ensemble-averaged extinction, C_{ext}, and scattering C_{sca}, cross sections per particle and the dimensionless Müller scattering matrix from equation (20). The process of the scattering is depicted by the following equation

$$I_{\text{sca}} = \frac{n\, C_{\text{sca}} dV}{4\pi R^2} \quad F(\Theta) I_{\text{inc}} \tag{21}$$

where Θ is the scattering matrix angle (angle between the incident and scattered beam), and $F(\Theta)$ is the Müller matrix. The Tmatrix model calculates both scattering and extinction cross sections C_{sca} and C_{ext}, respectively, single scattering albedo, asymmetry parameter, and the Stokes and Müller matrices.

The single scattering albedo of a particle is a measure of particle scattering cross section relative to its total extinction cross section (absorption plus scattering cross sections) and is mathematically defined by the equation (22) as follows

$$\omega = \frac{C_{\text{sca}}}{C_{\text{ext}}} = \frac{C_{\text{sca}}}{C_{\text{abs}} + C_{\text{sca}}} \tag{22}$$

Another important parameter which describes angular distribution of the scattered radiation is the phase function $P(\Theta)$ or the scattering phase function and it is defined as the scattered intensity at a certain angle Θ

$$P(\Theta) = \frac{I(\Theta)}{\int_0^{\pi} I(\Theta)\sin(\Theta)d(\Theta)} \tag{23}$$

where Θ is the scattering angle and I(Θ) is the intensity [6]. The Asymmetry parameter g is defined similarly as the intensity weighted average of the cosine of the scattering angle

$$g = \frac{1}{2}\frac{\int_0^{\pi} \cos(\Theta)\, I(\Theta)\sin(\Theta)\, d(\Theta)}{\int_0^{\pi} I(\Theta)\sin(\Theta)\, d(\Theta)} = \frac{1}{2}\int_0^{\pi} \cos(\Theta)P(\Theta)\sin(\Theta)d\Theta \tag{24}$$

where the factor 1/2 ensures values of g = 1 for light forward scattered completely at Θ = 0^o, and of g = -1 for light backward scattered completely at Θ = 180^o. On the other hand, a value of g = 0 indicates that the radiation is scattered isotropically.

Figures 5 and 6 show calculation of the Tmatrix model for both extinction and scattering cross sections, single scattering albedo, and asymmetry parameter in function of the effective radius at a wavelength of 0.870 μm. The model was run for a composite ensemble of particles, with refractive index of m = 1.68 + i0.31 for a high polluted day in February 09, 2009 [19]. Figure 5 show an increasing function of the scattering parameters. This is so, because the greater the effective radius (and in consequence, the area) the more the scattering or the extinction cross section of the particle. In addition, the values of single scattering albedo in figure 6 are related with the scattering and extinction cross section values for the composite particles and show some predominance of Mineral Dust. On the other hand, the asymmetry parameter plot of the same figure 6 indicates the tendency of the larger particles to scatter forward.

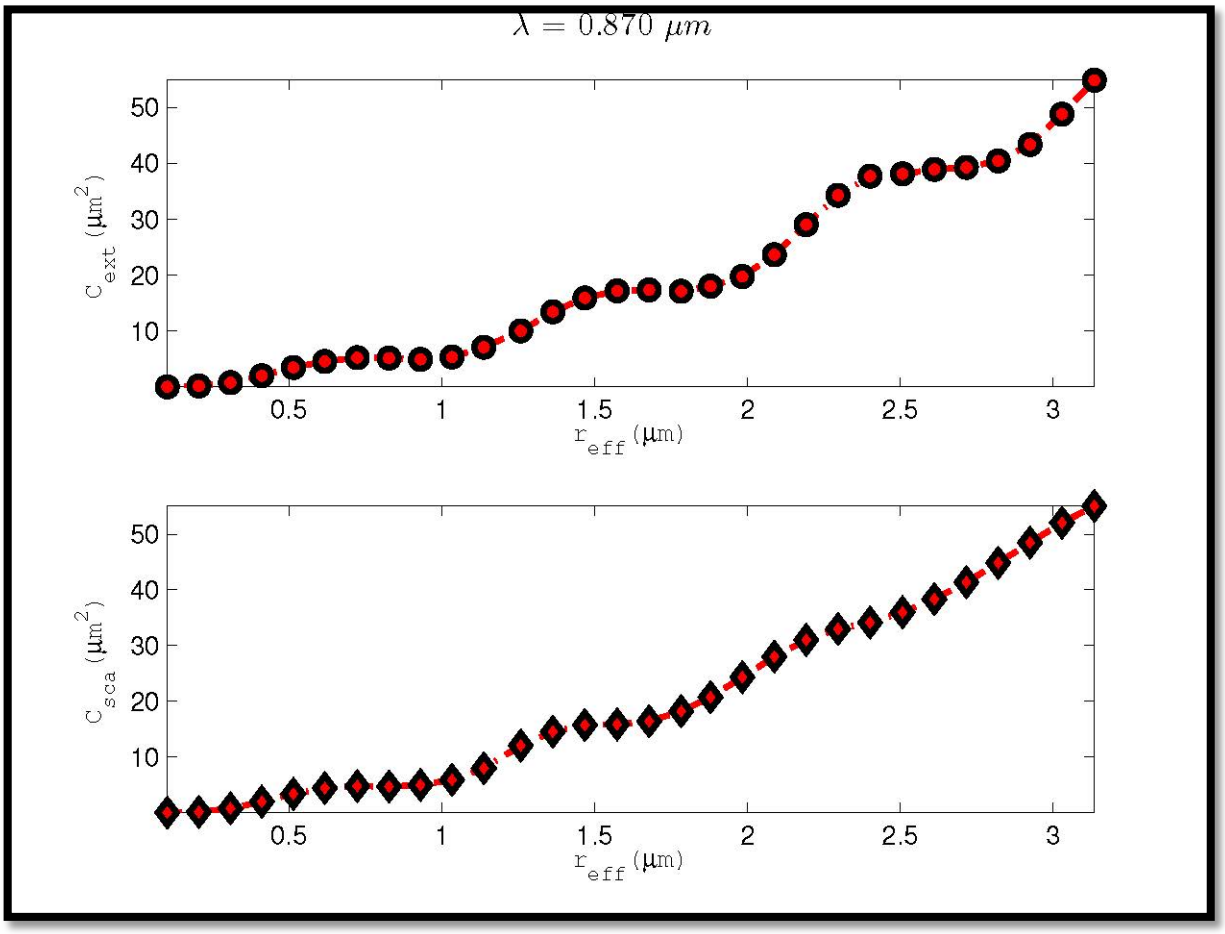

Figure 5: Some important parameters calculated with T-matrix in function of the effective radius of the scatterer particle. Top: extinction cross section, Bottom: scattering cross section.

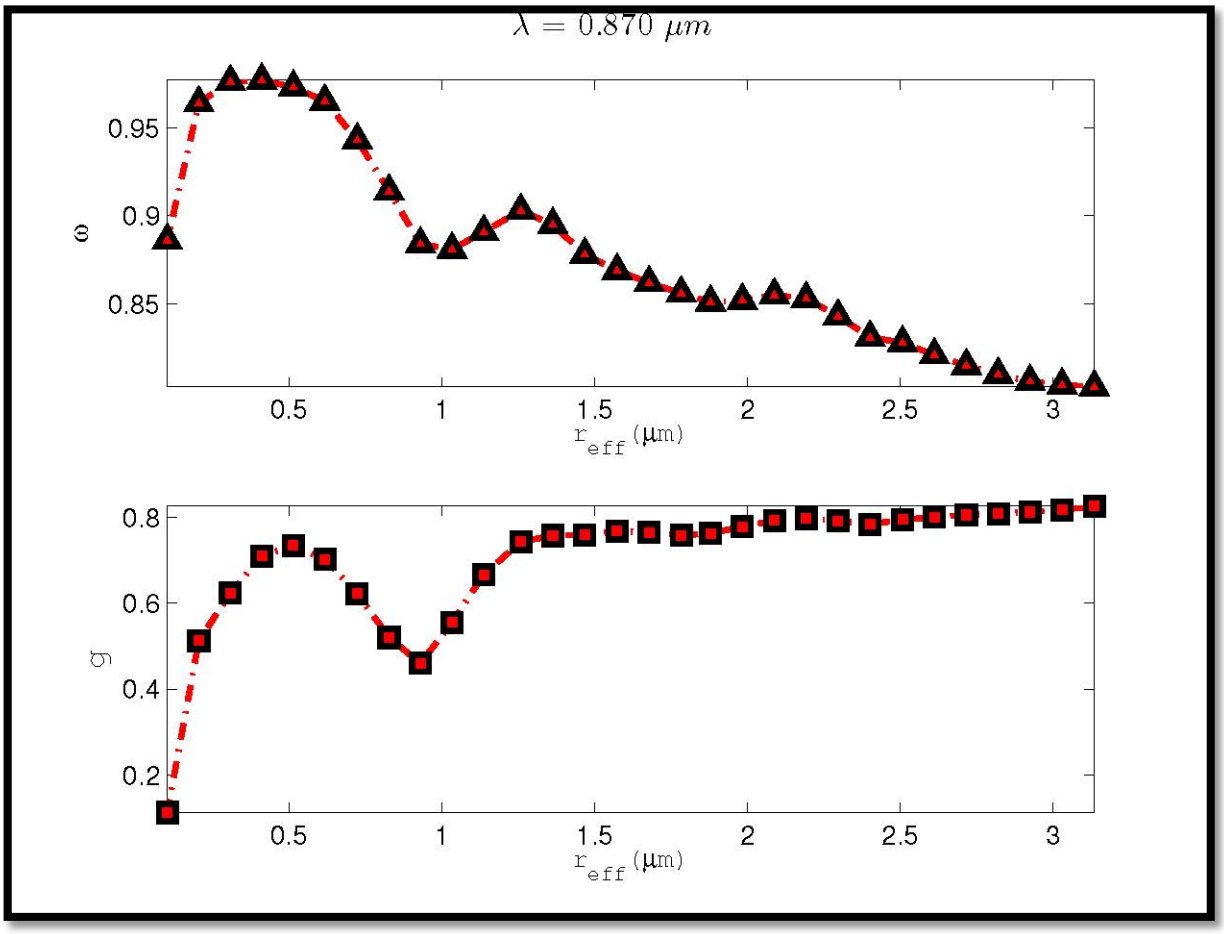

Figure 6: Some important parameters calculated with T-matrix in function of the effective radius of the scatterer particle. Top: single scattering albedo, and Bottom: asymmetry parameter.

1.4 VISIBILITY

Visibility is a measure of how far we can see through the air due to the optical properties of the atmosphere itself, the amount of distribution of light or the characteristic of the object at which we are to look. As it was stated in section 1.1, in the solar spectrum, the effect of gases on visibility are neglected in comparison with the effects of scattering and absorption by particles. A usual definition of visibility is the meteorological range. The meteorological range is a function of the contrast ratio, defined as

$$\beta_{\text{ratio}} = \frac{I_B - I}{I_B} \tag{25}$$

The contrast ratio gives the difference between the background intensity and the intensity of the viewer's line of sight, all relative to the ground intensity [3]. If the contrast ratio is zero, then an object cannot be differentiated from background light. If on the contrary the contrast ratio is unity, then an object is perfectly visible.

We define the liminal or threshold contrast ratio as the lowest visually perceptible brightness contrast a person can see. Then, the meteorological range is the distance from an object at which the contrast ratio equals the liminal contrast ratio of 0.02 (2%). Expressing the contrast radio as an exponential decay of the meteorological ratio

$$\beta_{\text{ratio}} = \frac{I_B - I}{I_B} = \mathrm{e}^{-\mathrm{B}_{\text{ext}} x} \tag{26}$$

and when β_{ratio}= 0.02 at a wavelength of 0.55 _m, the resulting distance *x* is the meteorological range (also called the Koschmieder equation).

$$x = \frac{3.92}{B_{\text{ext}}} \tag{27}$$

We will use the term visibility as the meaning of meteorological range along this work.

During high polluted day scenarios due to dust storm for example, the change in visibility is dramatic. To have a better idea of this effect, some pictures were taken at El Paso High School on March 19, and April 17 of 2013 during both a clean day and a high polluted day respectively. The visibility values on the figures 7, 8, 9, and 10 were also compared with visibility values from TheWeather Channel at http://www.timeanddate.com/weather/usa/el-paso.

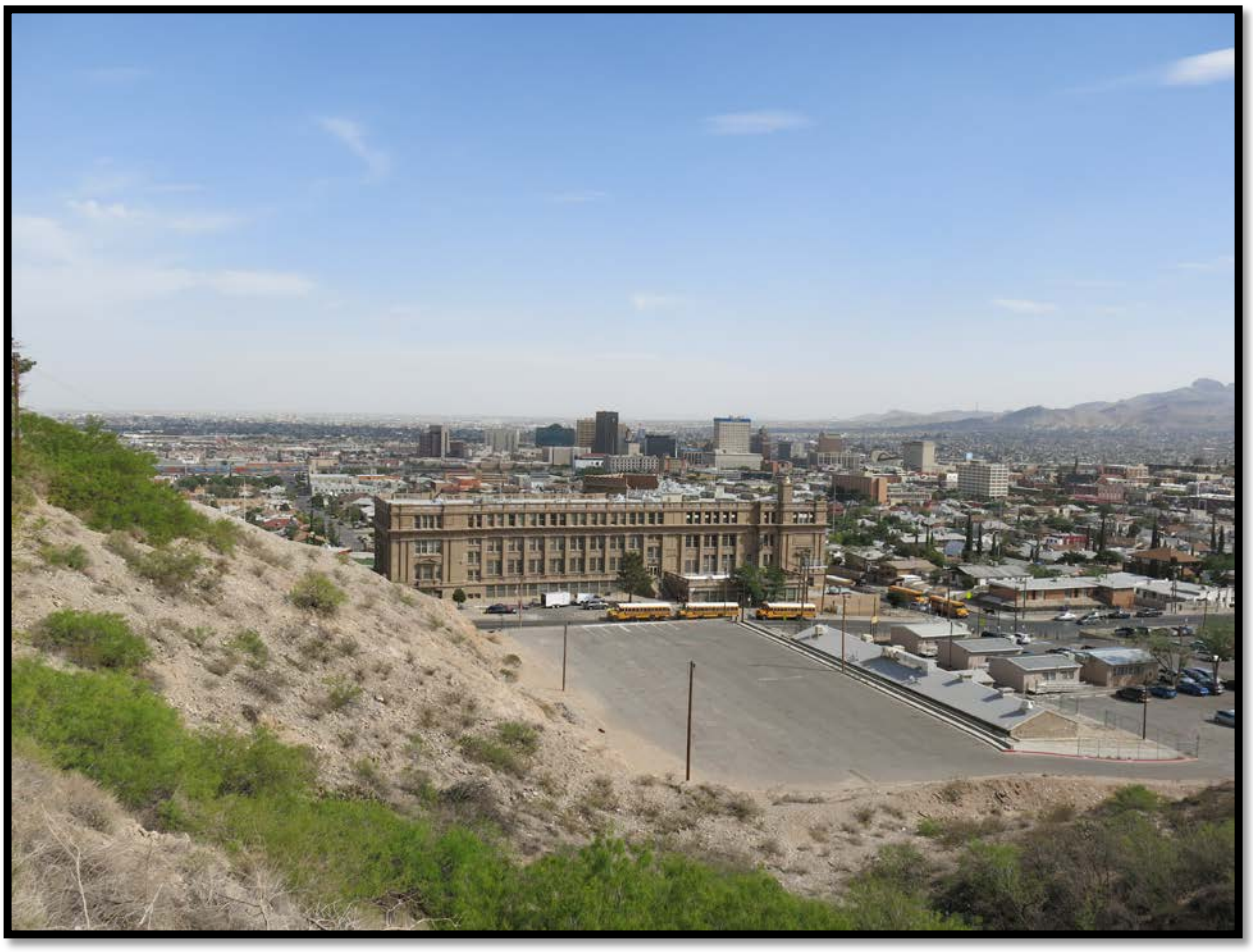

Figure 7: El Paso High School on clean day of March 19 of 2013.

Figure 8: El Paso High School on polluted day of April 17 of 2013.

Figure 9: El Paso High School tracking field on clean day of March 19 of 2013.

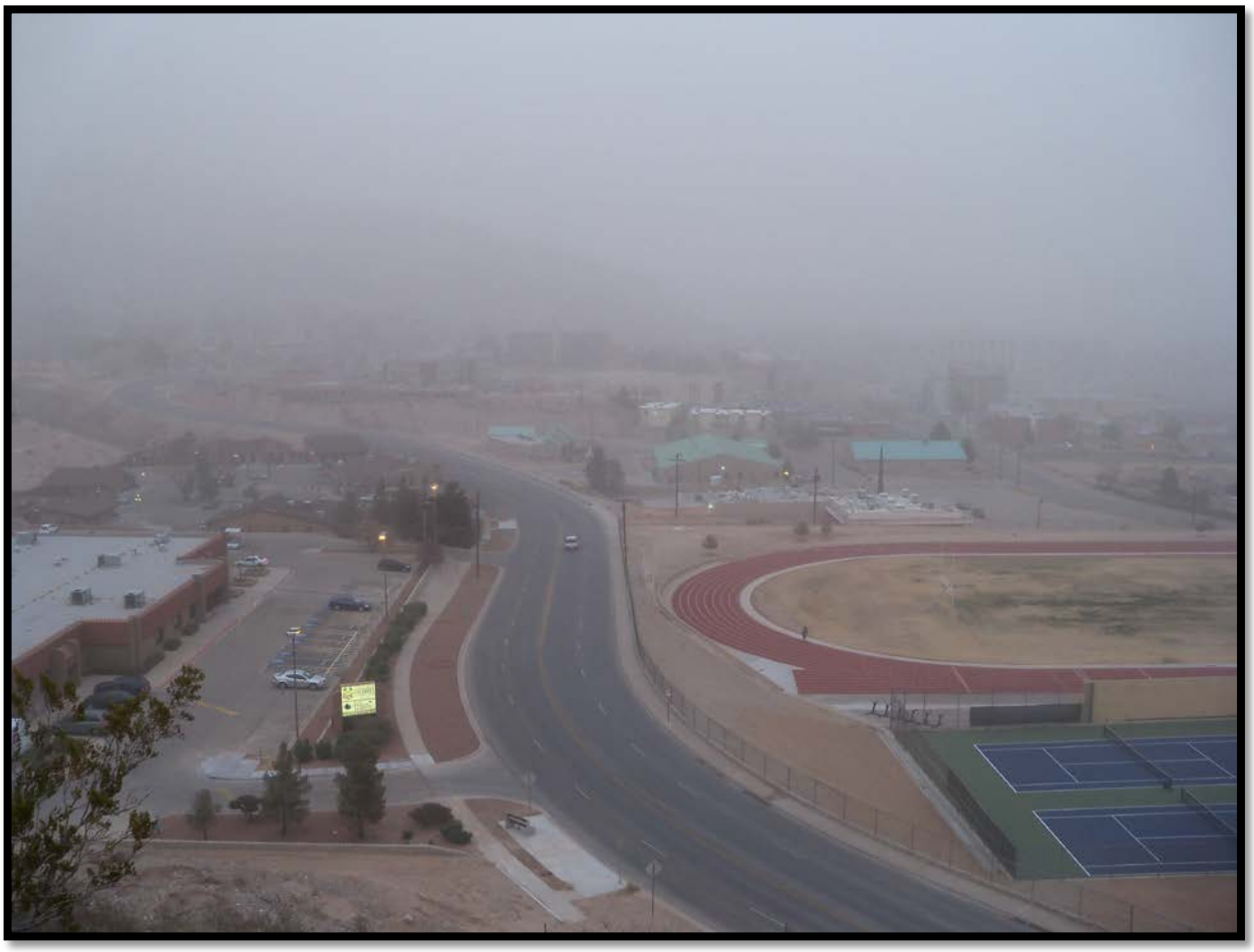

Figure 10: El Paso High School tracking field on polluted day on April 17 of 2013.

Chapter 2. Methodology

2.1 INSTRUMENTATION

In order to have an accurate description of the particles during the day, the Atmospheric Physics Laboratory acquired a laser particle counter model Climet CI150, which provides number distributions in four defined channels, and a Photoacoustic Extinctiometer, which provides scattering values, absorption and extinction coefficients, and detects soot at 870 nm. These instruments will be described in the next subsections as well as the mathematical model used to calculate the cross sections of the particles. At the end, the place selected to install the instruments for collecting data will also be described.

2.1.1 Optical particle laser counter

An optical particle counter uses a high-intensity light source (a laser), a controlled air flow (viewing volume), and a highly sensitive light photodetector [20]. The instrument measures the scattering of the light produced by the interaction of the laser with the air sample. The light scattered is converted to electric signals or electric pulses which are proportional to the pulses of scattered light which at the same time is proportional to the size of the particle. The next step procedure is to analyze the height of the electric signals. It is achieved by a pulse height analyzer which examines the magnitude of the electrical pulses and places the values into an appropriate sizing channel. The channels contain information about each pulse that correlates to particle sizes.

The laser particle counter instrument used in this work is the Climet CI-150t (Climet instrument 150t) which is a laser diode based aerosol particle counter that monitors particles in four ranges or bins: 0.3-0.5, 0.5-1.0, 1.0-5.0, and > 5.0 μm.

Figure 11: Climet CI-150t - Laser Particle Counter.

It is fully self-contained, operating on battery power or AC power for sampling convenience [21]. It works by taking samples at flow rates of air at one cubic foot per minute (1 CFM). The sample air is filtered before being exhausted through the rear panel. Counts of the types of particles are displayed and printed in a variety of formats. They can be stored on a 3.5" floppy disk or in the computer through a RS-232 serial port. Data are displayed as a comma delimited ASCII which contains the total count, differential count, concentration per cubic foot, and concentration per cubic meter. The instrument uses a highly efficient optical system and detection electronics based on a light scattering principle. The light from a 50 mW laser diode is scattered by the particles and then collected by an elliptical mirror and focused onto a solid state photo detector, which converts the light energy into electrical current. Figure 11 displays a picture of the instrument.

2.1.2 Photoacoustic Extinctiometer (PAX)

The Photoacoustic Extinctiometer (PAX) is a sensitive, high-resolution, fast response instrument for measuring aerosol optical properties relevant for climate change and carbon particle sensing [22]. Its applications are to air quality and visibility, atmosphere, health effects, combustion source emissions and biomass burning.

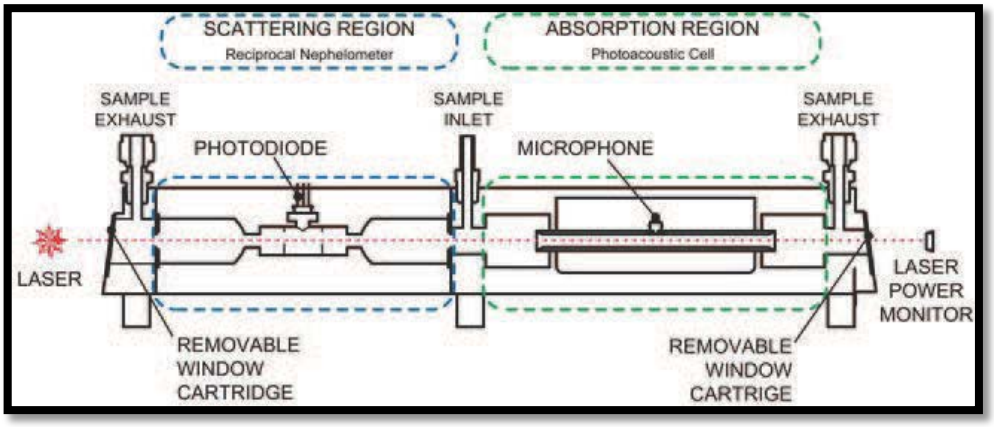

Figure 12: Photoacoustic extinctiometer circuit diagram.

Figure 13: Photoacoustic extinctiometer model PAX 870 nm.

Figure 12 depicts the internal mechanism of the instrument. It uses a modulated diode laser to simultaneously measure light scattering and absorption. The Atmospheric Physics Laboratory at the University of Texas at El Paso acquired the standard 870 nm wavelength which is especially sensitive to black carbon particles, since there is relatively little absorption from gases and non-BC aerosol species at this wavelength. Figure 12 shows the mechanism of measurement through the circuit diagram. A 1 liter per minute aerosol sample flow is drawn into the PAX using an internal vacuum pump controlled by two critical orifices, the inlet and exhaust orifices. The flow is split between the nephelometer and photoacoustic resonator for simultaneous measurement of light scattering and absorption. The absorption measurement uses in-situ photoacoustic technology. A laser beam directed through the aerosol stream is modulated at the resonant frequency of the acoustic chamber.

Absorbing particles heat up and quickly transfer heat to the surrounding air. The periodic heating produces pressure waves that can be detected with a sensitive microphone and determine aerosol light absorption. Additionally, the PAX uses a wide-angle integrating reciprocal nephelometer to measure the light scattering coefficient. The scattering measurement responds to all particle types regardless of chemical makeup, mixing state, or morphology.

2.1.3 The Visible Multifilter Rotating Shadowband Radiometer

The Visible Multifilter Rotating Shadowband Radiometer (Vis-MFRSR) instrument consist of a broadband channel together with a rotating shadowband which measures solar irradiance at six narrowband wavelengths (nominal 415, 500, 615, 673, 870, and 940 nm; each 10 nm FWHM) and instantaneous optical depth. These measurements are made every 15 seconds and integrated into 3-minute averages and stored by an on-board computer.

The University of Texas at El Paso, Texas, was integrated as one of the monitoring sites once it installed the Vis-MFRSR on January 6, 2006 on the roof of the Undergraduate Learning Center (UGLC) of the University of Texas at El Paso (UTEP) and started to collect data since then (See figure 14).

a b

Figure 14: Side (a) and close up view (b) of the Visible Multifilter Rotating Shadowband Radiometer installed at the roof of the Undergraduate Learning center (UGLC), at the University of Texas at El Paso.

2.2 MATHEMATICAL MODELS

2.2.1 The Tropospheric Radiative Transfer Model (TUV)

The TUV model version 5.0 is a one-dimensional radiative transfer code that uses either or both of Eddington's approximations and the discrete ordinate method to describe the radiative transfer through the atmosphere [23]. The code gives outputs of various spectral irradiances in the UV and visible spectra by using input data, such as geographic coordinates and atmospheric parameters in standard format. The Tropospheric Radiative Transfer Model, TUV, has been used to solve the Radiative Transfer Equation and obtain single scattering values as it will be explained in section 3.3.

2.2.2 The Tmatrix model

The Tmatrix model is a powerful tool that accurately computes light scattering by non-spherical particles. A very detailed description of the input values of the code is done by Mishchenko [24]. In this work, the Tmatrix version for randomly oriented non-spherical particles in double precision was modified and applied using the variables from table 2. The code was modified in order to obtain C_{ext} and C_{sca} values at the effective radius for the four bins of the laser particle counter at different wavelengths and different refractive indexes as is indicated in table 3. All input parameters must be specified in the same units. If the units we are working on are based on lengths like micrometers ($1\mu m = 10^{-6}m$), then all the derivatives of length like area and volume must be expressed in micrometers. Tables 2 and 3 describe some input and output values respectively from the code.

Table 2: Tmatrix input parameter values

Input	**Value**	**Description**
R1 and R2	R_i	Array of 4 bins
ICHOICE	2	Gauss Elimination for inverse matrices
NDISTR	2	Lognormal distribution
DDELT	0.001	Accuracy
NPNA	19	Number of scattering angles
NKMAX	5	Number Nr of Gaussian quadrature points
LAM	0.87	LAM varies from 0.3-0.94 μm
EPS	1.0	For sphere particles a/b=1.00
RAT	0.5	Equal surface area sphere radius
NP	-1	For spheroides

The model outputs the coefficients for the generalized spherical functions which are related with the solution of the scattering problem for the wave equations (16a) and (16b), however only the values of scattering and extinction cross sections, the single scattering albedo and the asymmetry parameter are going to be used in the computation of the optical coefficients and visibility. There are also other important outputs that need to be defined.

The average area of the geometric projection per particle $\langle G \rangle$

$$\langle G \rangle = \int_{r_{min}}^{r_{\max}} dr\, n(r) \pi r^2 \tag{28}$$

The average area of the geometric projection per particle $\langle V \rangle$

$$\langle V \rangle = \int_{r_{min}}^{r_{\max}} dr\, n(r) \frac{4}{3} \pi r^3 \tag{29}$$

The average radius $\langle R \rangle$

$$\langle \mathrm{R} \rangle = \int_{\mathrm{r_{min}}}^{\mathrm{r_{max}}} \mathrm{dr\ n(r)} \tag{30}$$

where n(r) is the number distribution of the particles (particles/cm3), and r is the radius of the particle.

2.3 THE VOLUME-WEIGHTED METHOD

The volume-weighted method [25] is a technique which calculates the refractive indexes by knowing the mass fraction and density of the species of a composite medium. The method is shown in equations (31) and (32). The mean refractive index ($\bar{n} = \bar{m} + i\bar{k}$) is computed with the real refractive index for species $j(m_j)$, the mass fraction of each species $j(X_j)$, and the species density (ρ_j, g/cm^3).

The mean imaginary part of the complex refractive index is computed using the value corresponding to each species (k_j)

$$\bar{n} = \bar{\rho} \sum_j \frac{X_j m_j}{\rho_j} + i\,\bar{\rho} \sum_j \frac{X_j k_j}{\rho_j} \tag{31}$$

the mean density $\bar{\rho}$, is computed with

$$\bar{\rho}^{-1} = \sum_j \frac{X_j}{\rho_j} \tag{32}$$

Table 3: Tmatrix output information

Output	**Description**
R1 and R2	Minimum and maximal radii, respectively
REFF	Effective radius
VEFF	Effective variance
CEXT	Ensemble-averaged extinction cross section per particle
CSCA	Ensemble-averaged scattering cross section per particle
COS	Ensemble-averaged asymmetry parameter
ALBEDO	Ensemble-averaged single scattering albedo
<G>	Averaged projected area
<V>	Averaged volume per particle
<R>	Averaged radius

2.4 SINGLE SCATTERING ALBEDO, AND EXTINCTION COEFFICIENTS

The characterization of the relative contributions of particle scattering and particle absorption to the total extinction by particles (scattering plus absorption) the single scattering albedo is used. The

aerosol single scattering albedo (ω_{aer}) is also defined as the measure of particle scattering coefficient relative to the total extinction coefficient by particles (absorption plus scattering coefficients). This definition is similar to equation (22), except that in that case the cross sections were used. The equation that describes this parameter is

$$\omega_{\mathrm{aer}} = \frac{B_{\mathrm{sca}}}{B_{\mathrm{ext}}} = \frac{B_{\mathrm{sca}}}{B_{\mathrm{abs}} + B_{\mathrm{sca}}} \tag{33}$$

2.5 SITE SELECTION

Both instruments, the laser particle counter and the photoacoustic extinctiometer require a wide and clean protected area. The instruments are located at the Atmospheric Physics Laboratory of the University of Texas at El Paso. Both are installed following the proper technical criteria and connected to the roof through individual hoses especially designed to take air samples without friction. They are also protected from rain and snow to obtain clean samples during the data acquisition. The clean days were free cloud selected to avoid screening on illumination and also with low humidity conditions to avoid particle coating. For the polluted days, there were not specific restrictions at all. Most of the dusty day scenarios did not have rain activities and it was important to have the most data during the day for better analysis.

Chapter 3. Results and Discussion

3.1 SELECTION OF REPRESENTATIVE DAYS

Several cases for the determination of the scattering and extinction coefficients were calculated for both, polluted and unpolluted days. Since the start of the measurements with our instruments in the year 2013 until the day when this work was finished, there were registered six dust storm scenarios with our extinctiometer, they were in February 20, February 24, March 4, March 23, April 13, and April 17.

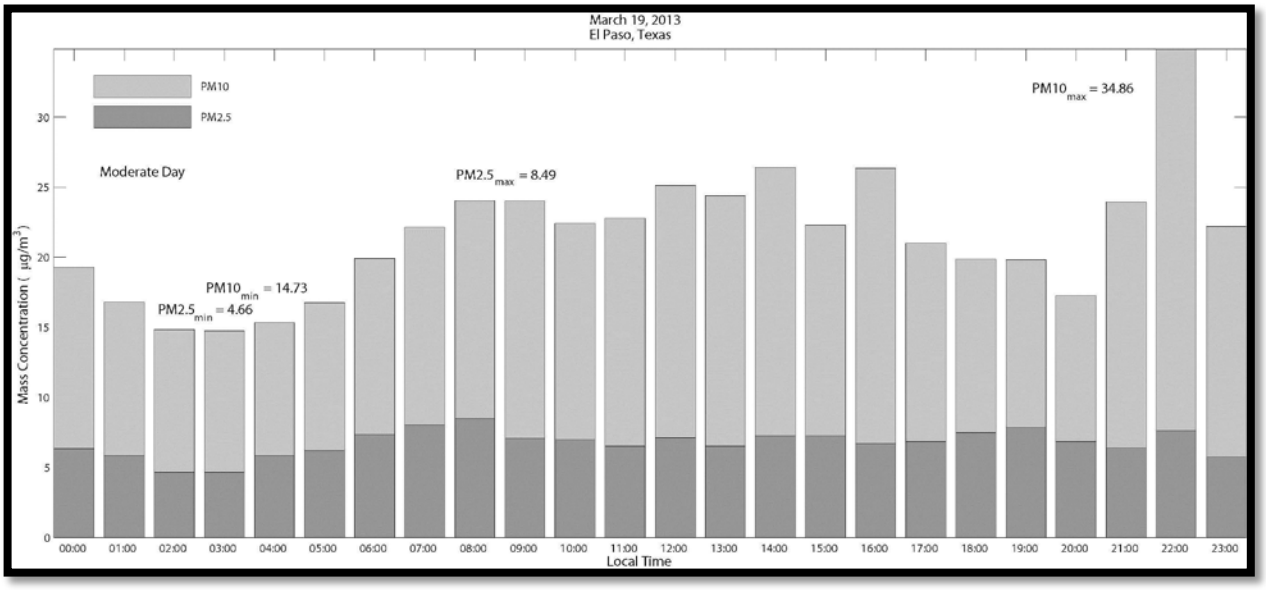

Figure 15: Low polluted day aerosol mass concentration (µg/m^3) on March 19, 2013.

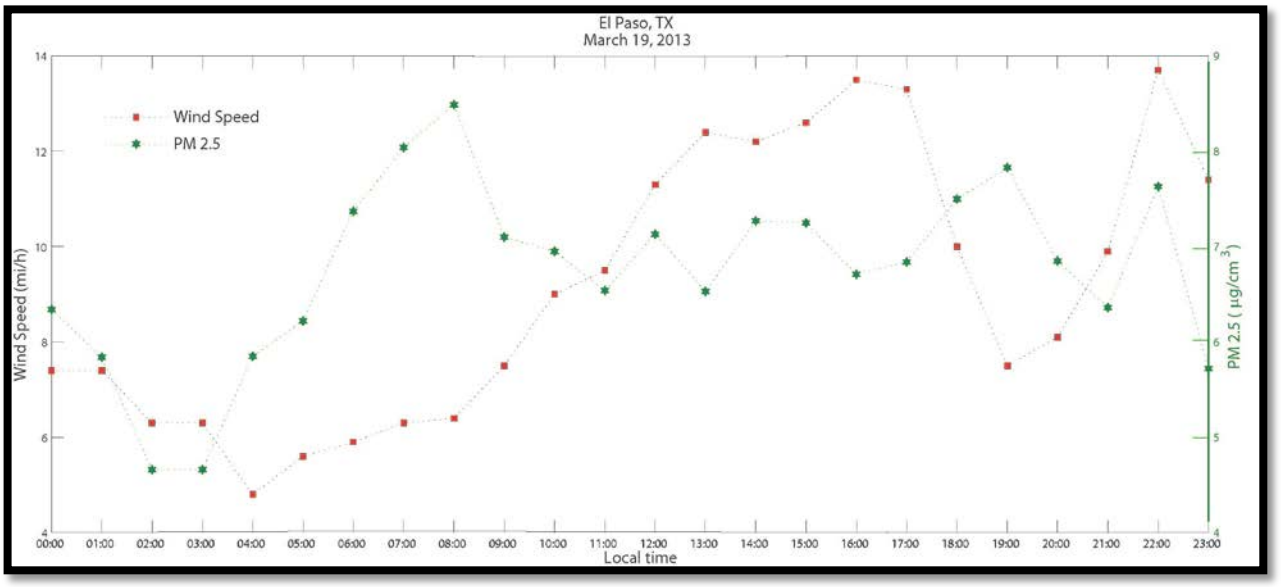

Figure 16: Wind speed (mi/h) and PM2.5 mass concentration (μg/cm3)

for low polluted day on March 19, 2013.

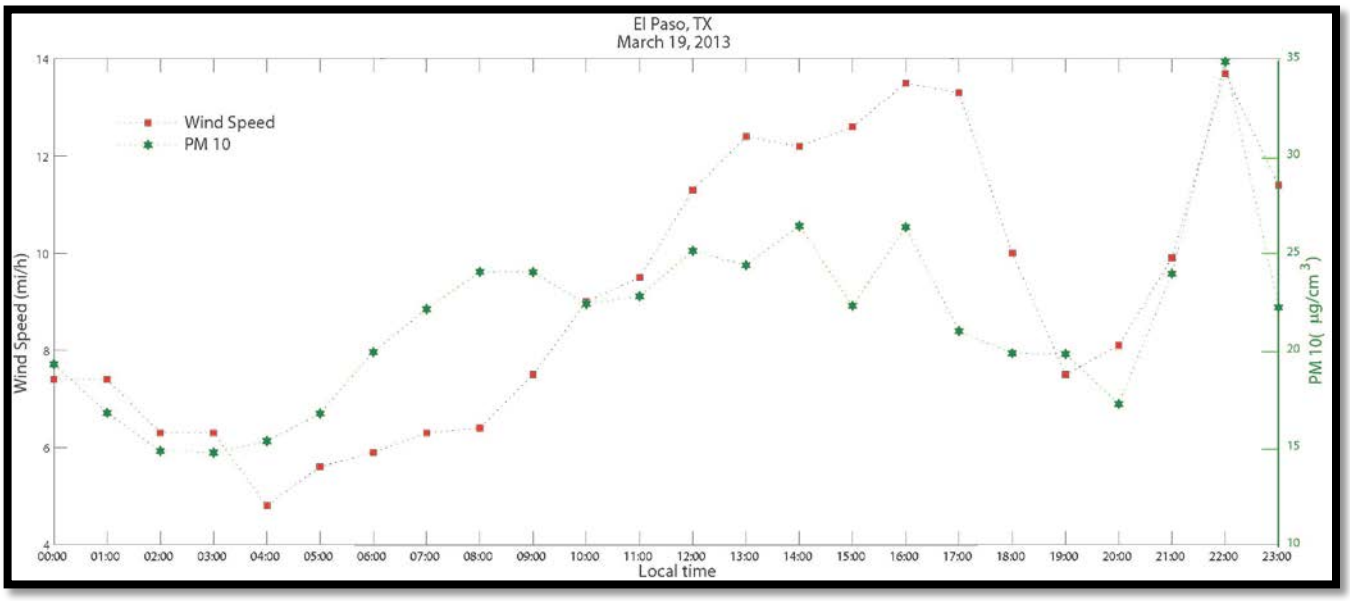

Figure 17: Wind speed (mi/h) and PM10 mass concentration (μg/cm^3) for low

polluted day on March 19, 2013.

The high concentration of particulate matter (μg/cm^3) with diameters of 2.5 and 10 μm (PM2.5 and PM10 respectively) were plotted for both low polluted and high polluted day scenarios. March 19,

2013 was a day of low mass concentration of aerosols having minimum and maximum of PM2.5 equals to 4.66 and 8.49 μg/cm^3 respectively. The minimum and maximum values for PM10 were 14.73 and 34.85 μg/cm^3 respectively. These values are depicted in figure 15 along with values of wind speed for this day. In figures 16 and 17, we observe that the values of wind speed for the clean day March 19, 2013 was between 5 to 13.5 miles per hour.

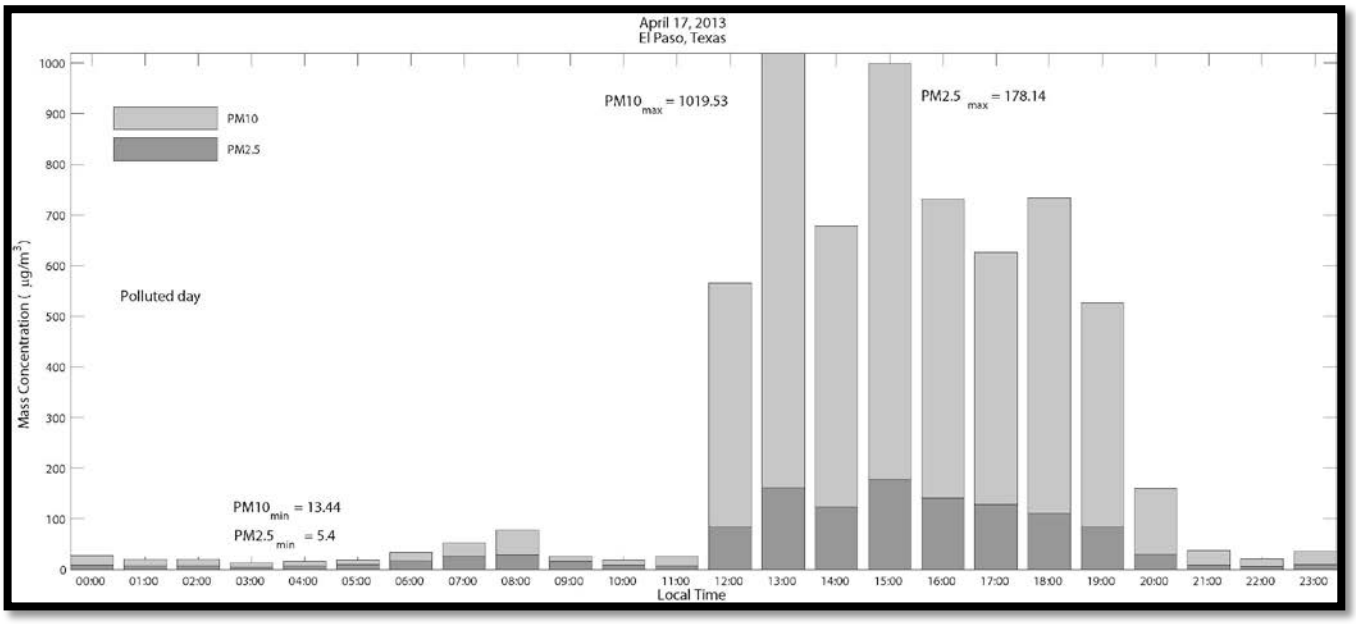

Figure 18: High polluted day aerosol mass concentration (μg/m^3) on April 17, 2013 (observe the scale of values for this day and compare with figure 15.

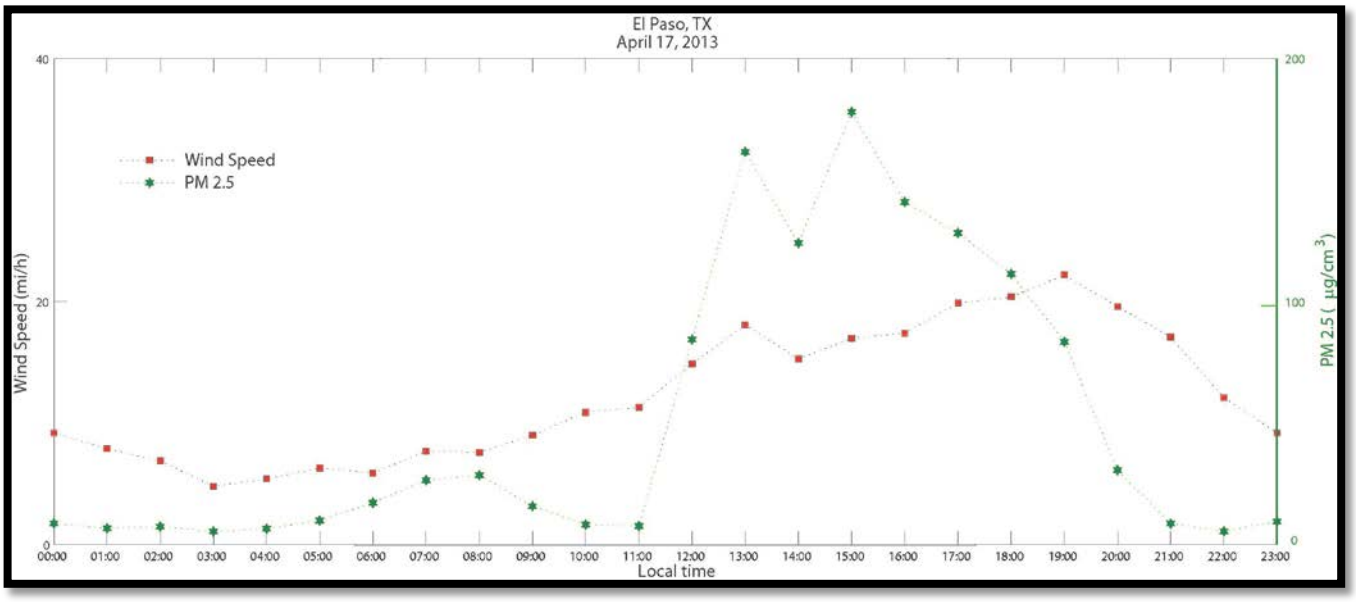

Figure 19: Wind speed (mi/h) and PM2.5 mass concentration (μg/cm^3) for high polluted day on April 17, 2013.

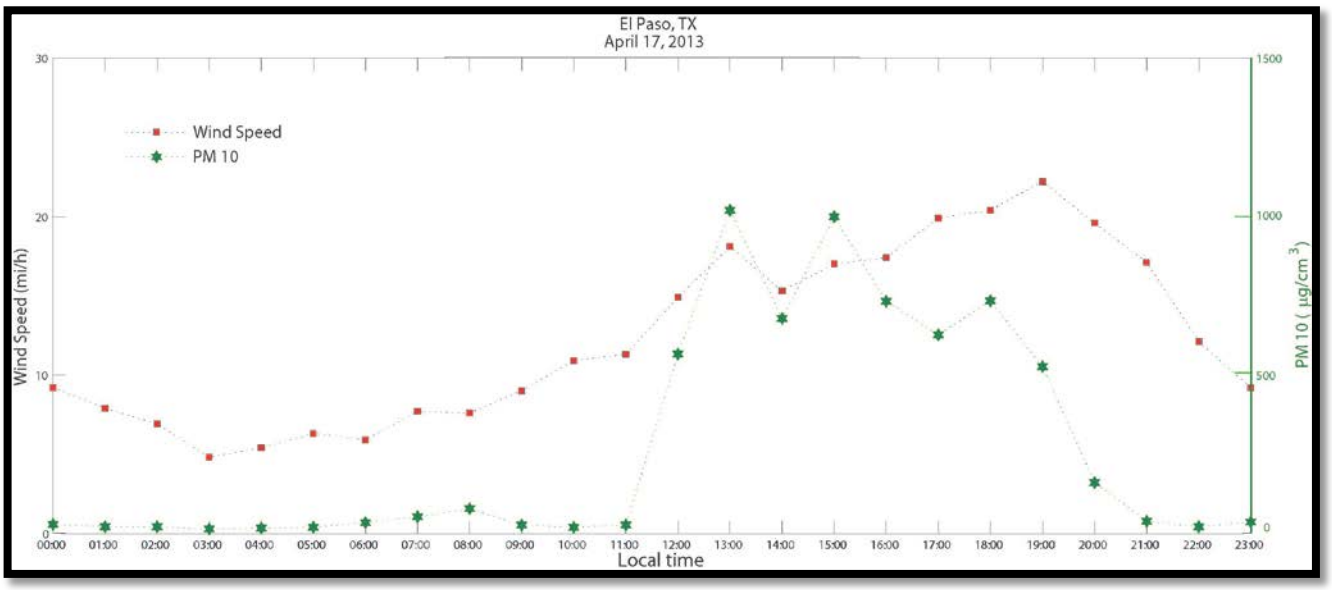

Figure 20: Wind speed (mi/h) and PM10 mass concentration (μg/cm^3) for high polluted day on April 17, 2013.

On figure 18, the maximum and minimum values for the particle mass concentration for the polluted day on April 17, 2013 for PM2.5 were 5.4 and 178.14 μg/cm^3 for minimum and maximum values respectively, while the PM10 minimum and maximum values were 13.44 and 1019.53 μg/cm^3 respectively. Additionally, the representation of wind speed for this polluted day was plotted in figures 19 and 20. Notice that the values of wind speed are related with the increase of the particulate matters mass concentration.

3.2 COMPUTATION OF B_{SCA}, B_{ABS}, AND B_{EXT}

Values of the scattering and extinction cross sections were calculated with the model. Number concentration of the particles were obtained from the laser particle counter at their four channels and then processed to express them in the units of particles/μm^3. The scattering and extinction coefficients were obtained by using the formula

$$B_{\text{sca}} = \sum_{i=0}^{N_B} n\, C_{\text{sca}} \tag{34a}$$

$$B_{\text{ext}} = \sum_{i=0}^{N_B} n\, C_{\text{ext}} \tag{34b}$$

where N_B is the number of bins of the particle counter, and the values for B_{sca} was obtained directly from the equation

$$B_{\text{abs}} = B_{\text{ext}} - B_{\text{sca}} \tag{35}$$

Equations (34a), (34b), and (35) are valid for scattering by individual or ensemble of particles and the single-scattering theory can be used even in the more concentrated atmospheric conditions if the average distance between particles is large compared to the particle size [6].

Each coefficient value was calculated with the model and then compared with the ones from the acoustic extinctiometer per hour at $\lambda = 0.87\mu m$ by using percent relative error

$$\delta_{(B)} = \frac{B_{\text{PAX}} - B_{\text{Model}}}{B_{\text{PAX}}} \tag{36}$$

where the coefficients labeled correspond to B_{abs}, B_{sca}, and B_{ext} to either the model or the extinctiometer. The values of $\delta_{(B)}$ from equation (36) less or equal to 1% were kept and saved to produce the figures 21, 22, 23 for the low-polluted day, and figures 24, 25, and 26 for the polluted day.

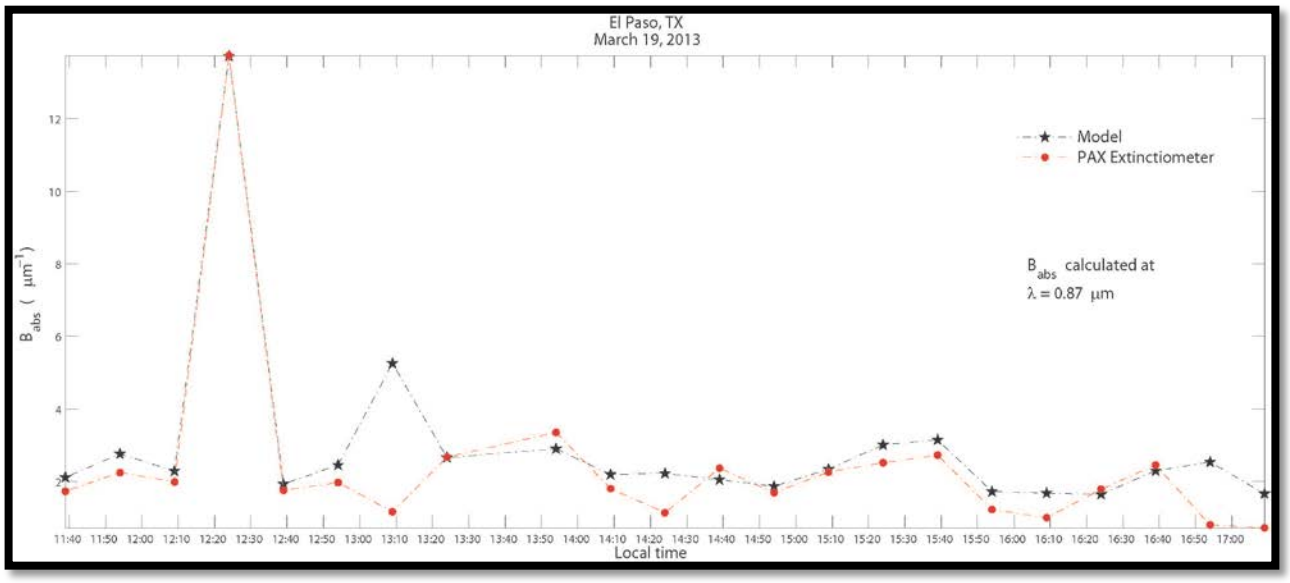

Figure 21: Absorption coefficient values calculated with Tmatrix and compared with the acoustic extinctiometer at 0.87μm for March 19 of 2013.

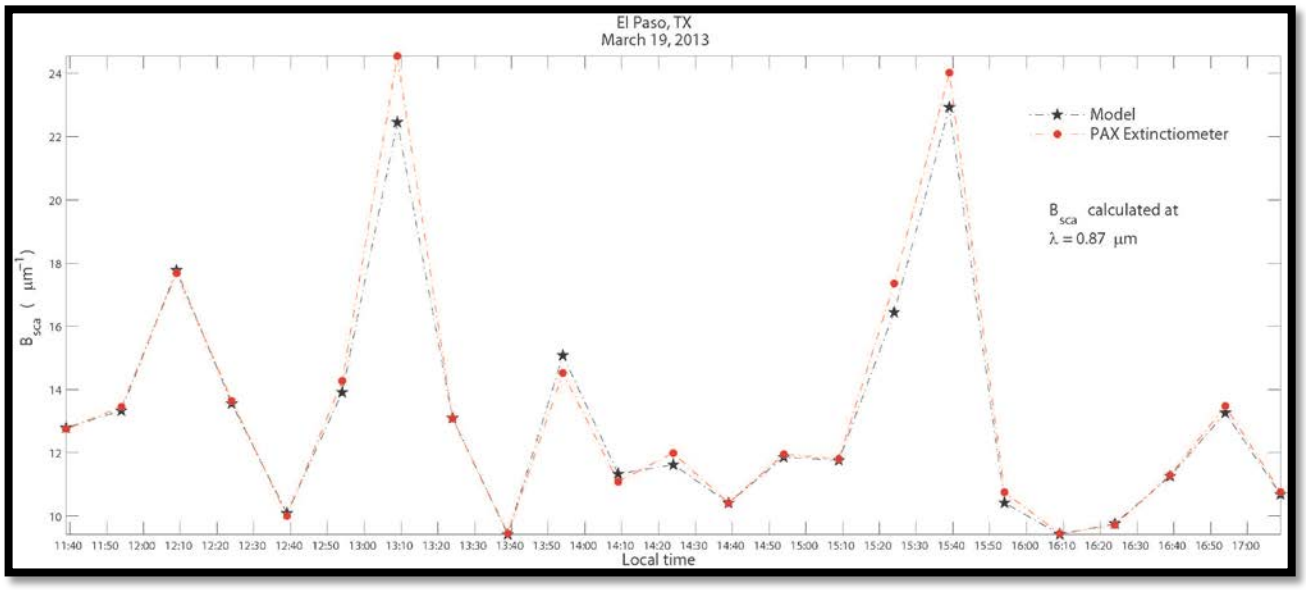

Figure 22: Scattering coefficient values calculated with Tmatrix and compared with an acoustic extinctiometer at 0.87μm for March 19 of 2013.

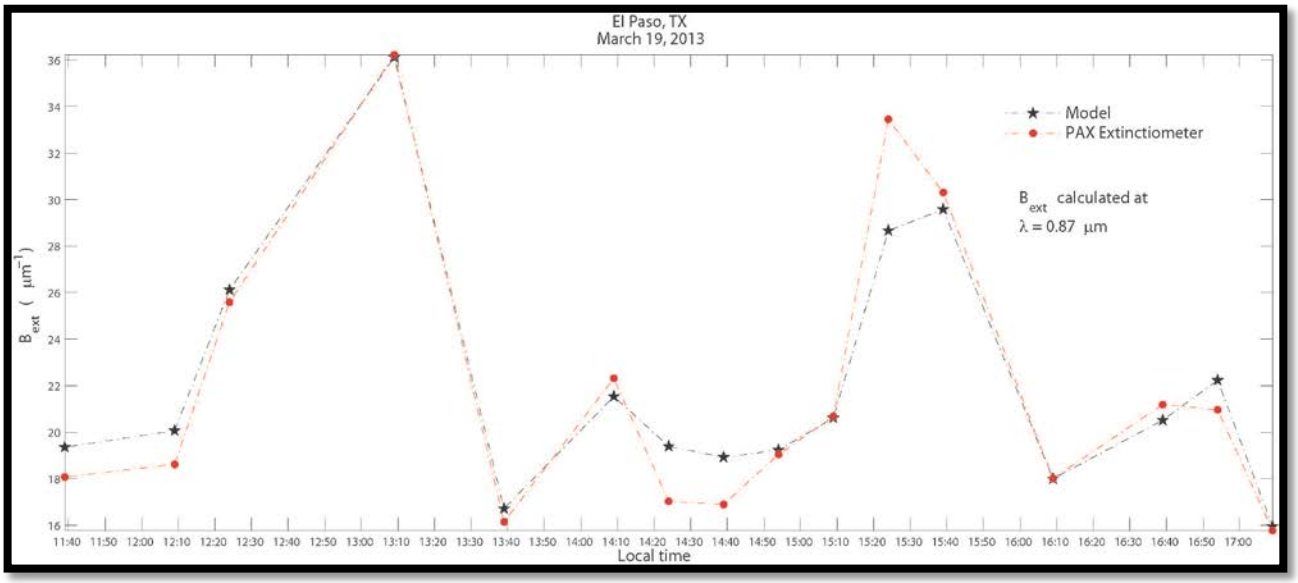

Figure 23: Extinction coefficient values calculated with Tmatrix and compared with the acoustic extinctiometer at 0.87μm for March 19 of 2013.

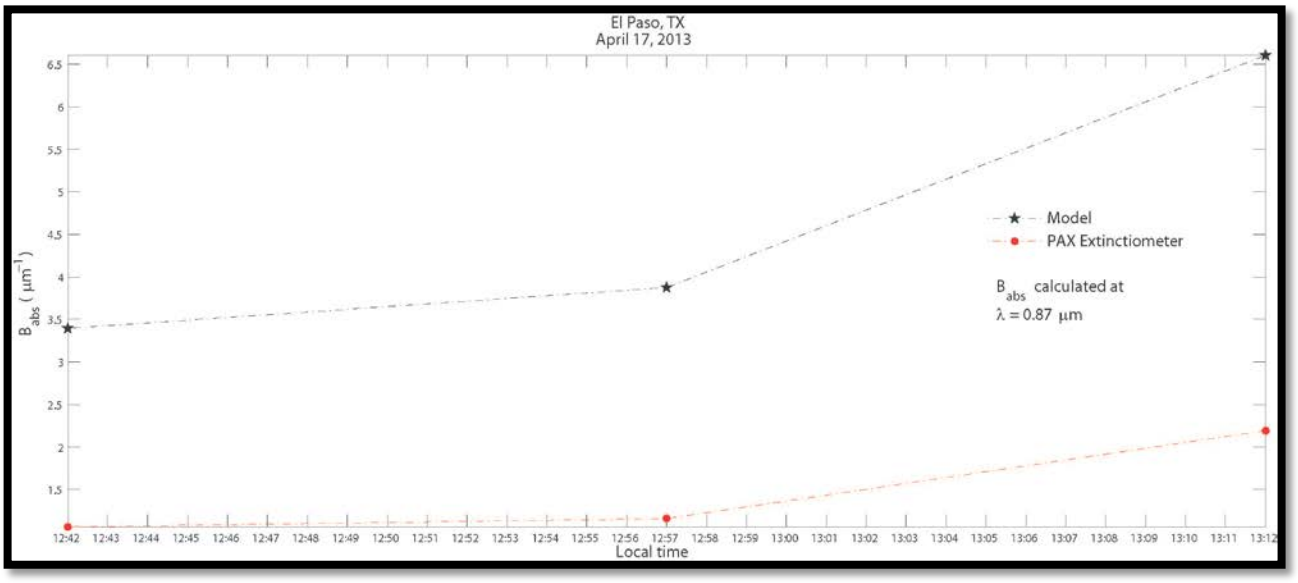

Figure 24: Absortion coefficient values calculated with Tmatrix and compared with an acoustic extinctiometer at 0.87μm for April 17 of 2013.

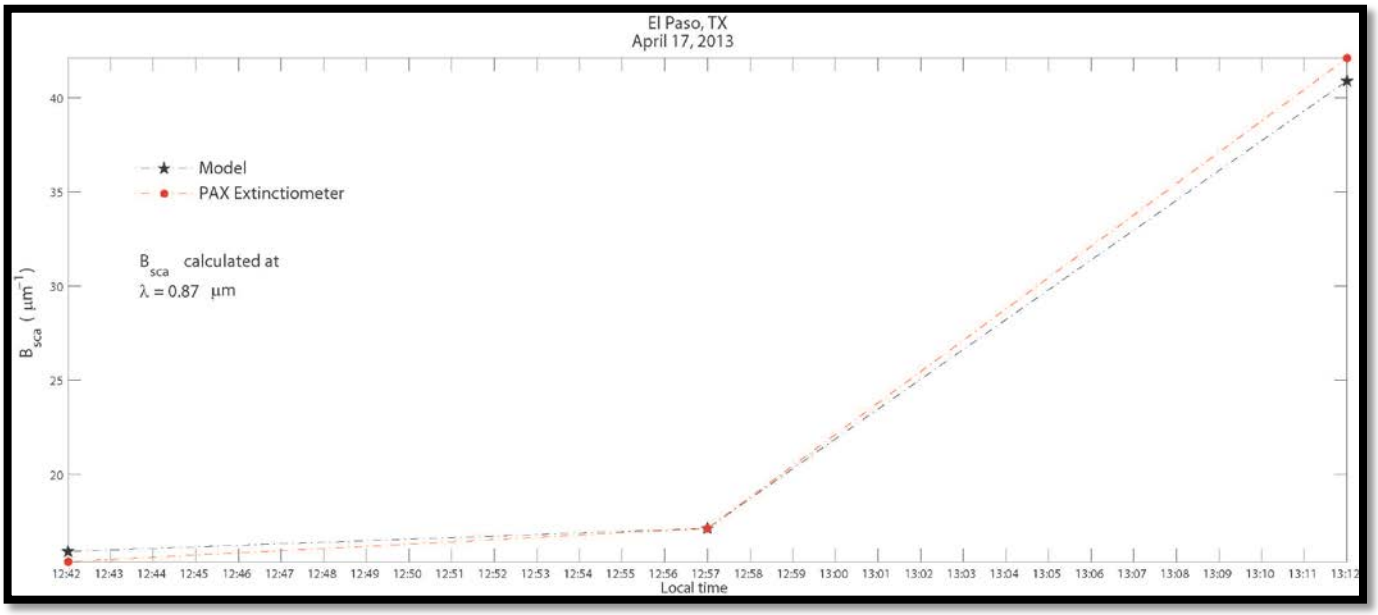

Figure 25: Scattering coefficient values calculated with Tmatrix and compared with an acoustic extinctiometer at 0.87μm for April 17 of 2013.

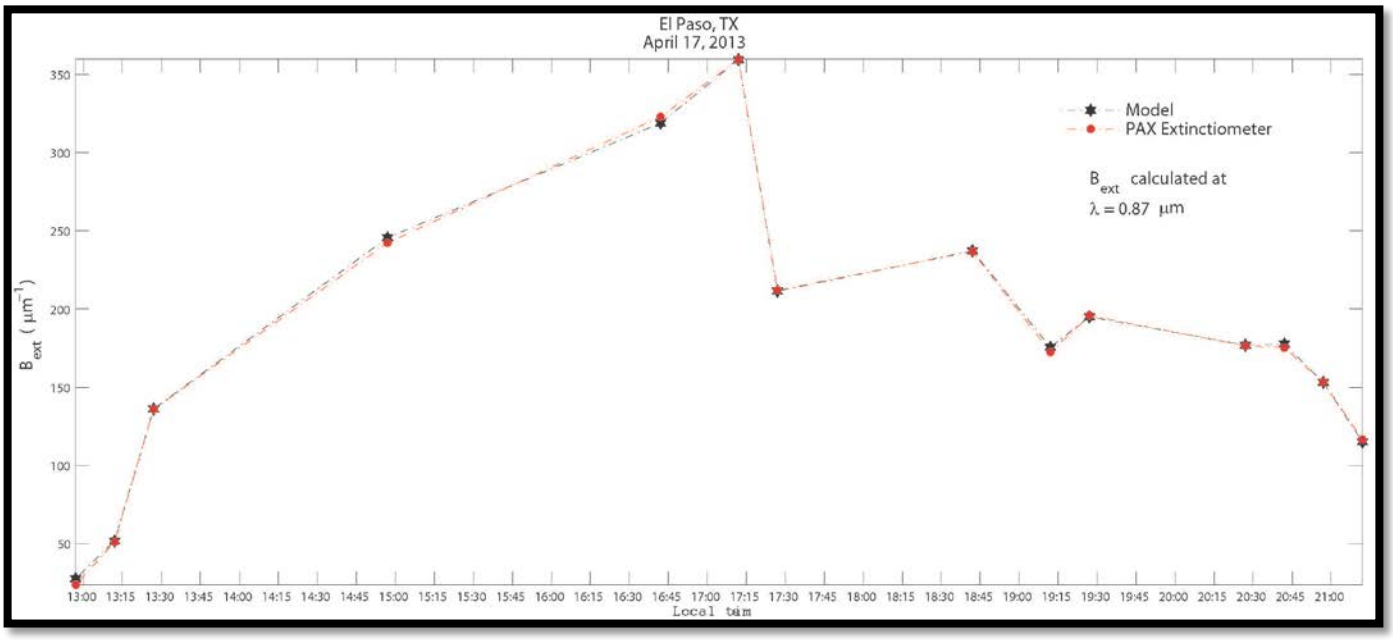

Figure 26: Extinction coefficient values calculated with Tmatrix and compared with an acoustic extinctiometer at 0.87μm for April 17 of 2013.

3.3 SINGLE SCATTERING ALBEDO RETRIEVALS

Values of single scattering albedo were retrieved for the wavelengths of 0.87 μm by using the direct-to-diffuse (DDR) method. This method consists of changing the values of ω_{aer} in the TUV code to obtain outputs of direct-to-diffuse irradiance ratios and comparing them against values obtained from the Visible-MFRSR instrument using error percent relative error $\delta_{(SSA)}$, as is shown in the following equation

$$\delta_{(SSA)} = \frac{\left|DDR_{Vis(MFRSR)} - DDR_{TUV}\right|}{DDR_{Vis(MFRSR)}} \tag{37}$$

This method was published in 2012 [26].

In both cases, scattering most frequently occurs than absorption during those days. For the low polluted day, March 19th of 2013, high values of scattering were observed during the day and a decrease

in single scattering albedo (decreasing of scattering also) at 13:30 hours afternoon was observed. This behavior is consistent with the soot detection by the photoacoustic extinctiometer and by the model at 12:24 hours as it can be observed in figure 27, where the largest peak of the absorption graph indicates high contribution of soot at that time. For the polluted day, values of single scattering albedo increase. This is in correspondence with the pollutant composition, which most of them are mineral dust. For the high polluted day of April 17, 2013, it can also be observed in figure 28, the presence of scattering during the day, even when the mass concentration was high due to the dust storm (see figures 19 and 20), indicating the presence of more scattering particles in our region during daylight. Figure 28 also shows an increment of absorptive particles during the night and early morning.

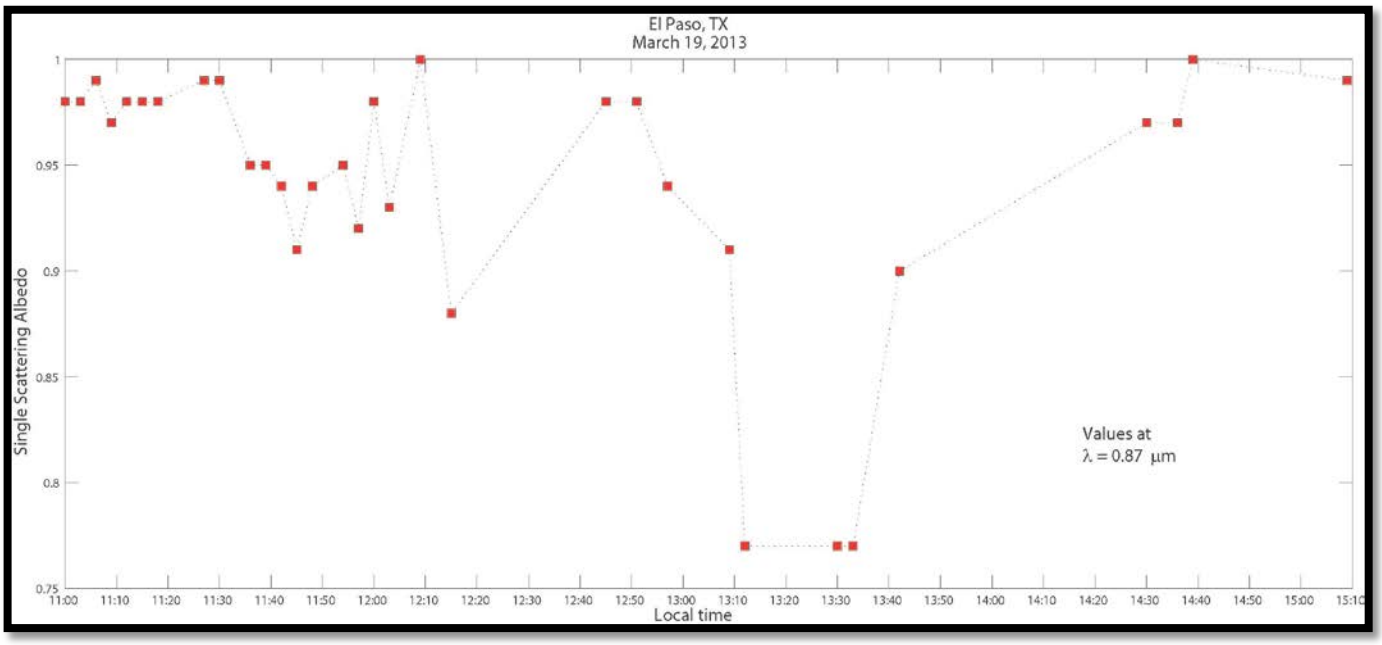

Figure 27: Single scattering albedo values retrieved at 0.87μm for March 19 of 2013.

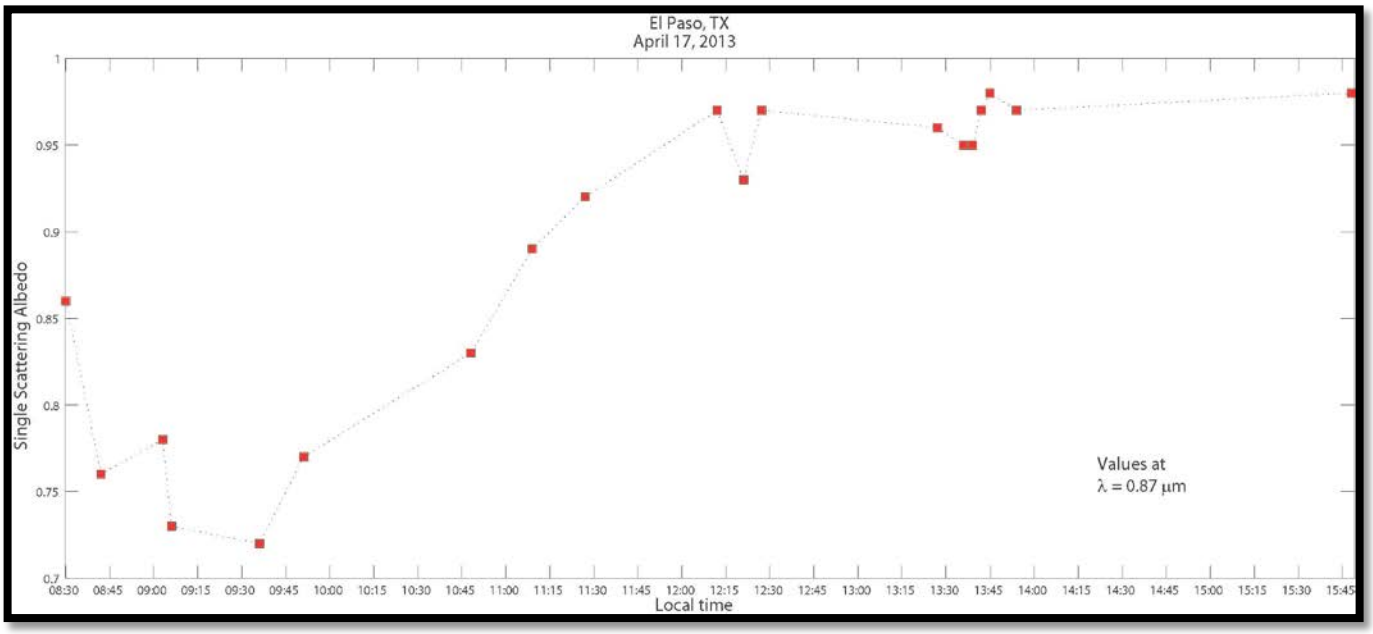

Figure 28: Single scattering albedo values retrieved at 0.87μm for April 17 of 2013.

3.4 COMPUTATION OF THE MASS FRACTION OF SPECIES AND CORRESPONDING REFRACTIVE *N*REF

Due to the complex topography and location of the mountains and river valley in the El Paso del Norte region, it results in a constrained air basin where, on calm days, especially in the winter, anthropogenic air pollution is trapped over the metropolitan area [27]. On windy days, especially during the winter and early spring, mineral dust and sand blowing out of the surrounding desert causes high particulate matter concentrations [28].

Table 4. Physical constant of species used in refractive index and density calculations

(courtesy, Hand, J. L., et al. [2])

Species	Density (g/cm^3)	Refractive index
H2SO4	1.8	1.408
NH4HSO4	1.78	1.479
(NH4)3H(SO4)2	1.83	1.527
(NH4)2SO4	1.76	1.531
Organic Carbon	1.4	1.55
Elemental Carbon	2.0	1.96-0.66i
NaNO3	2.261	1.587
SiO2	2.32	1.486
Al2O3	3.97	1.765
Fe2O3	5.24	3.011
CaO	3.3	1.833
MgO	2.58	1.735
TiO2	4.23	2.58

Table 5: Percentage of species during the low polluted day March 19, 2013.

Time	**n_{ref}**	**Soot(%)**	**Mineral Dust(%)**
11:39	1.570 + i 0.088	0.1	0.9
11:54	1.609 + i 0.165	0.0	1.0
12:09	1.530 + i 0.008	0.2	0.8
12:24	1.843 + i 0.631	1.0	0.0
12:39	1.749 + i 0.445	0.6	0.4
12:54	1.570 + i 0.088	0.1	0.9
13:09	1.570 + i 0.088	0.1	0.9
13:24	1.872 + i 0.689	0.8	0.2
13:39	1.872 + i 0.689	0.8	0.2
13:54	1.570 + i 0.088	0.1	0.9
14:09	1.609 + i 0.165	0.0	1.0
14:24	1.609 + i 0.165	0.0	1.0
14:39	1.813 + i 0.571	0.8	0.2
14:54	1.570 + i 0.088	0.1	0.9
15:09	1.646 + i 0.239	0.2	0.8
15:24	1.570 + i 0.088	0.1	0.9
15:39	1.530 + i 0.008	0.2	0.8
15:54	1.609 + i 0.165	0.0	1.0
16:09	1.872 + i 0.689	0.8	0.2
16:24	1.646 + i 0.239	0.2	0.8
16:39	1.781 + i 0.509	0.7	0.3
16:54	1.609 + i 0.165	0.0	1.0
17:09	1.570 + i 0.088	0.8	0.2

Table 6: Percentage of species during the polluted day April 17, 2013.

Time	$\mathbf{n_{ref}}$	Soot(%)	Mineral Dust(%)
13:12	1.749 + i 0.445	0.6	0.4
13:27	1.681 + i 0.310	0.3	0.7
14:57	1.781 + i 0.509	0.7	0.3
16:42	1.609 + i 0.165	0.0	1.0
17:12	1.681 + i 0.310	0.3	0.7
18:42	1.609 + i 0.165	0.0	1.0
19:12	1.781 + i 0.509	0.7	0.3
19:27	1.609 + i 0.165	0.0	1.0
20:27	1.609 + i 0.165	0.0	1.0
20:42	1.781 + i 0.509	0.7	0.3
20:57	1.646 + i 0.239	0.2	0.8

In conclusion, it is stated that the two main components of the air for the El Paso del Norte region is soot and mineral dust. The main component of soot is elemental carbon with density of ρ= 2.0 g/cm^3. Mineral dust has many components, and for this region the density and refraction index was assumed as a simplified composition of 90% SIO_2 9% $CaCO_3$, and 1% Fe_2O_3. The densities and refractive indexes values were obtained from table 4.

The volume-weighted averaged method was used to find the mass fraction of the species and from there derive the refractive index of the composite medium in the air. By expanding equation (31) and comparing their respective real and complex indices to the one calculated with the Tmatrix code, we have found the following mass fractions and refractive indexes for both low-polluted and high-polluted days. From the results in table 5 which correspond to the low polluted day, it is important to notice that our method describes the refractive indexes and the percentage of the species. For example if we

observe at 12:24 all the aerosols detected belong to soot, the refractive index is high for scattering and absorption and it is expected a high peak at that time for B_{abs}. Indeed, if we look at figure 21, the peak is pronounced there. We can observe the same for refractive index values of B_{sca} at 12:09, 13:09, and 15:39 where there are three big peaks as is shown in figure 22.

By using the equation (36) and figure 23, we can observe the contribution of these values in the extinction coefficient. The analysis for the polluted day was more complicated. The rapid variation of the number concentrations during the dust storm changed the composition very fast and the equation (36) was not accurate, providing only few values for the scattering and absorption coefficients as it is observed in figures 25 and 24 respectively. However, from table 6, we can observe some important results when comparing figure 26. The peak at 17:12 from the figure shows a high value in extinction, which from the table 6 corresponds to important contributions of the scattering coefficients and mass fraction of mineral dust. Soot also contributed to the effects on visibility when its mass concentration is high. During that polluted day especially after 3:00 PM when the dust storm moved large masses of air and pollutants, but it is more likely that most of the particles are mineral dust.

3.5 VISIBILITY CALCULATION WITH THE KOSCHMIEDER EQUATION

As it was defined, visibility values were obtained directly from the extinction coefficient and then used in equation (27). It was not possible to compare values with experimental data. However, the modeled calculations were compared with the concentration of PM2.5 and PM10 values. The figures 29 and 30 show us the effect of these particles in values of visibility for a low polluted day and figures 31 and 32 show us the effect of these particles on a high polluted day scenario.

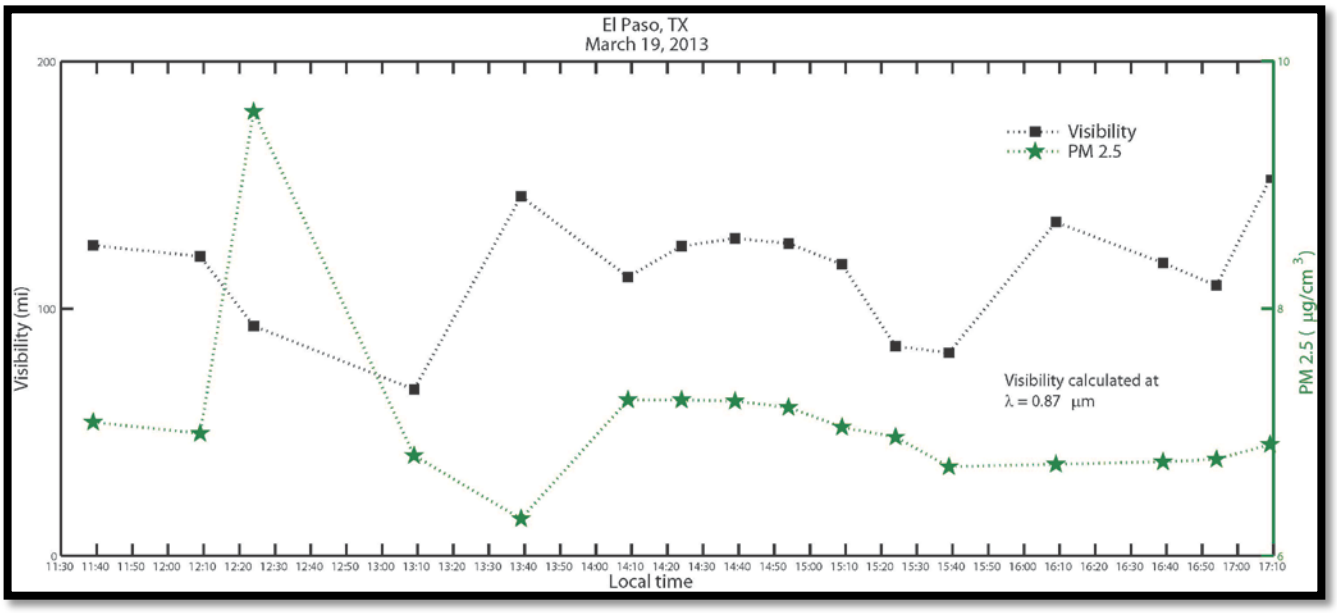

Figure 29: Particulate matter of 2.5 μm of diameter and its effects in visibility for a low polluted day scenario on March 19 of 2013.

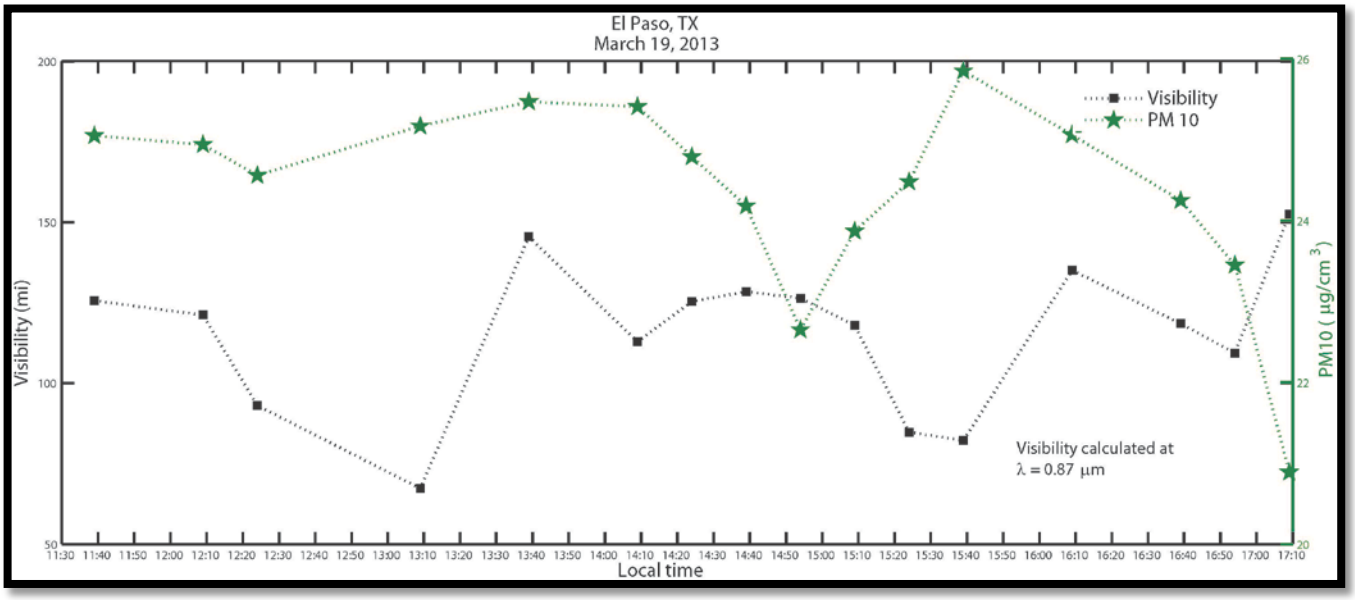

Figure 30: Particulate matter of 10μm of diameter and its effects in visibility for a low polluted day scenario on March 19 of 2013.

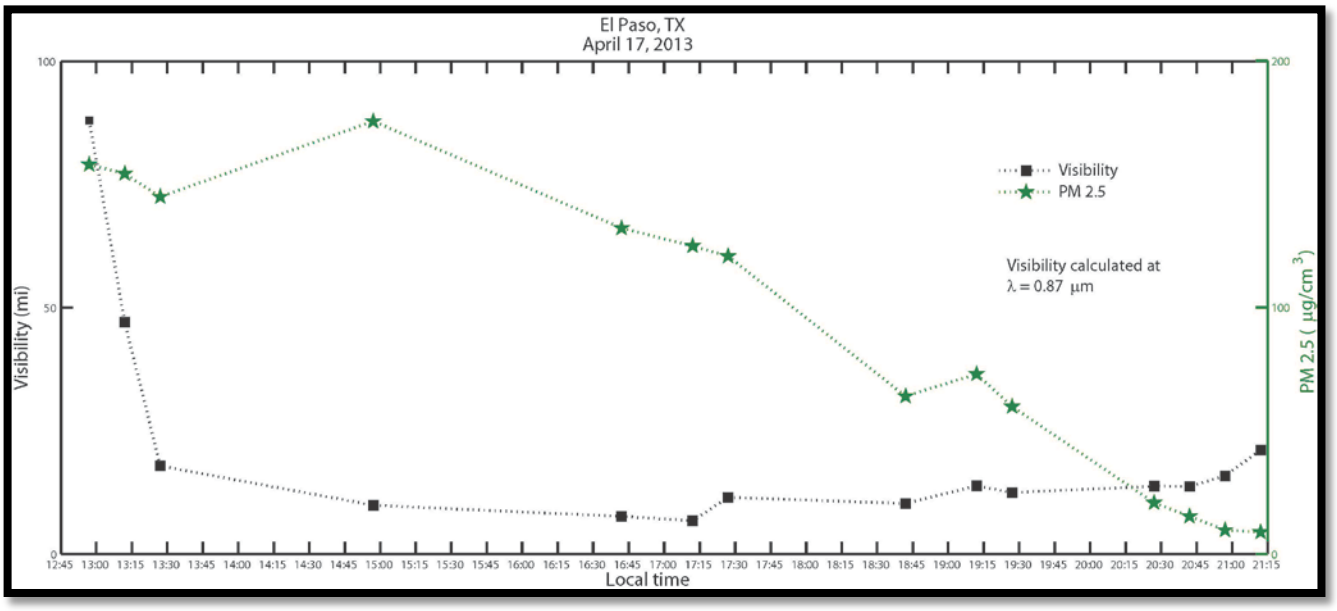

Figure 31: Particulate matter of 2.5 μm of diameter and its effects in visibility for a high polluted day scenario on April 17 of 2013.

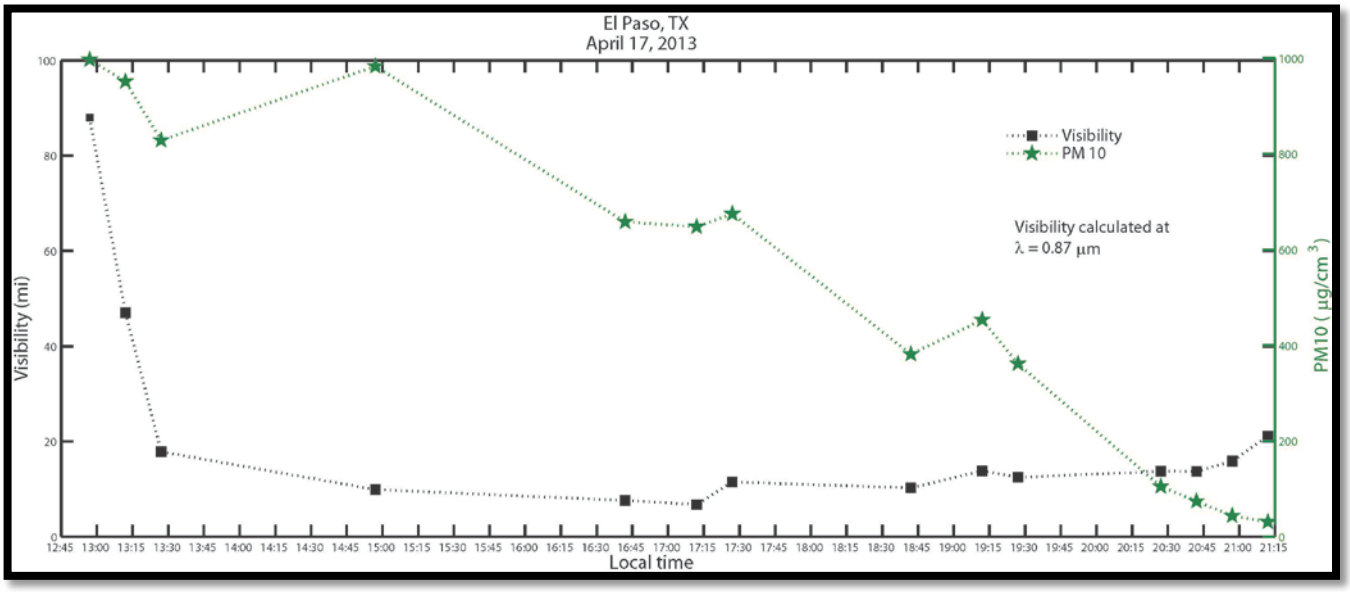

Figure 32: Particulate matter of 10 μm of diameter and its effects in visibility for a high polluted day scenario on April 17 of 2013.

Chapter 4. Conclusions and Future Work

4.1 Conclusions

A new methodology to model visibility was developed and applied to the El Paso del Norte Region.

The selected days corresponded to a low level polluted and a high level polluted day scenarios. The study was made by using the Tmatrix model to calculate cross sections and B_{ext}, B_{sca}, and B_{abs} coefficients.

Values of the extinction, scattering an absorption coefficients were compared with the photoacoustic extinctiometer at 0.87 μm showing good agreement.

The developed methodology was also used to find the composite refractive index for both day scenarios and estimate the percentages of the aerosol components.

The retrieval values of single scattering albedo from the visible MFRSR radiometer were used and correlated with the extinction results of the Tmatrix model.

This correlation showed the presence of more scattering particles in our region at the wavelength of 0.87 μm and the detection of absorptive particles during mid-day, in agreement with Medina, et al., 2012 [26]. These absorptive values correspond to the presence of soot.

4.2 Future Work

In this work it was assumed for the size distribution function of the particle counter that all the cases corresponded to the lognormal distribution, however this distribution may change during the day, and a least square routine to select the best distribution is suggested.

Some computation improvements will demand some cost of memory, processing, and time. The Tmatrix model has also a parallel version, which was developed to make bigger calculations. It is advisable to review the routines created and explore the capabilities of the model for larger data.

In the calculation, it was assumed that most of the particles were spherical or rounded in shape. In reality the shape of the particles can vary from spherical to non-spherical (also, chevyshev particles with more complicated shape).

Finally, we are trying to complement this work with some image processing of the pictures taken by ordinary digital cameras. In the future we expect to have this information as a data source for brightness and contrast information of the meteorological range or visibility.

References

[1] A. Kokhanovsky, Light Absorption and Scattering by Particles in the Atmosphere. Springer, 2008.

[2] J. L. Hand and S. M. Kreidenweis, “A new method for retrieving particle refractive index and effective density from aerosol size distributions data", Aerosol Science and Technology, vol. 10, pp. 1012-1026, 2002.

[3] M. Z. Jacobson, Fundamentals of Atmospheric Modeling. Cambridge University Press, 2005.

[4] C. F. Bohren and D. R. Hu_man, Absorption and Scattering of Light by Small Particles. Wiley-VCH, 1998.

[5] A. Winkel and G. Jander, Schewbsto_e in Gasen (Aerosole). Ferdinand Enke, 1939.

[6] H. J. Seinfeld and N. P. Spyros, Atmospheric Chemistry and Physics, from Air Pollution to Climate Change. John Wiley & Sons Inc., 2006.

[7] J. T. Peterson and C. E. Junge, Sources of particulate matter in the atmosphere, Man's impact on Climate. MIT Press, 1971.

[8] L. Elterman, “UV, Visible, and IR attenuation for altitudes to 50 km", Air Force Cambridge Res. Lab., vol. 68, 1968.

[9] A. P. Waggoner, R. E. Weiss, N. C. Ahlquist, D. S. Covert, S. Will, and R. J. Charlson, “Optical characteristics of atmospheric aerosols," Atm. Env., vol. 15, pp. 1891-1909, 1981.

[10] I. M. Mishchenko, Scattering, Absorption, and Emission of Light by Small Particles. Cambridge University Press, 2002.

[11] J. D. Jackson, Classical Electrodynamics. Wiley, 1975.

[12] H. C. van de Hulst, Light scattering by small particles. Wiley, 1957.

[13] E. Collett, Polarized Light: Fundamentals and Applications. CRC Press,1992.

[14] S. Chandrasekhar, Radiative Transfer. Dover Publications, 1960.

[15] P. C. Waterman, “Matrix formulation of electromagnetic scattering", Proc. IEEE, vol. 41, pp. 1633-1639, 1965.

[16] P. C.Waterman, “Symmetry, unitarity, and geometry in electromagnetic scattering", Phys. Rev., vol. D3, pp. 825-839, 1971.

[17] P. C. Waterman, Numerical solution of electromagnetic scattering problems. In Computer Techniques for Electromagnetics. R. Mitra, 1973.

[18] P. C. Waterman, “Matrix methods in potential theory and electromagnetic scattering", J. Appl. Phys., vol. 50, pp. 4550-4566, 1979.

[19] A. Esparza, R. Fitzgerald, T. Gill, and J. Polanco, “Use of light-extinction method and inverse modeling to study aerosols in the paso del norte airshed", Atm. Env., vol. 45, pp. 7360-7369, 2011.

[20] P. M. Systems, 2011, basic Guide to Particle Counters and Particle Counting.

[21] D. Aldaco and J. C. Roque, CI-550, laser particle counter, operator's manual. CLIMET INSTRUMENTS, 2002.

[22] D. M. Technologies, 2013, PAX, Photoacoustic Extinctiometer.

[23] S. Madronich, S. J. Flocke, and I. Petropavlovskikh, “Tropospheric ultraviolet - visible model (TUV)", Jan. 1997, National Center for Atmospheric Research NCAR Technical Note.

[24] M. I. Mishchenko and L. D. Travis, “Capabilities and limitations of a current fortran implementation of the tmatrix method for randomly oriented, rotationally symmetric scatterers", J. Quant. Spectrosc. Radiat. Transfer, vol. 60, pp. 309-324, 1998.

[25] J. L. Hand, S. M. Kreidenweis, J. Slusser, and G. Scott, “Comparisons of aerosol optical properties derived from sun photometry to estimates inferred from surface measurements in big bend national park, texas", Atm. Env., vol. 38, pp. 6813-6821, 2004.

[26] R. Medina, R. Fitzgerald, and Q. Min, “Retrieval of the single scattering albedo in the el paso-juarez airshed using the tuv model and a uv-mfrsr radiometer", Atm. Env., vol. 46, pp. 430-440, 2012.

[27] R. Pearson and R. Fitzgerald, \Application of a wind model for the el Paso-Juarez Airshed", J. of the Air and Wasted Management Association, vol. 51, pp. 669-680, 2001.

[28] N. Rivera Rivera, T. Gill, K. Gebhart, J. Hand, M. Bleiweiss, and R. M. Fitzgerald, “Application of a wind model for the El Paso-Juarez Airshed", Atm. Env., vol. 43, pp. 347-354, 2009.

Vita

Richard Medina Calderon was born in Trujillo, La Libertad, Peru. The fifth son of Bartolo Medina Avila and Dolores Calderon Aranda, he earned the bachelor degree in Physics from The Universidad Nacional Mayor de San Marcos in Lima, Peru, in the spring of 2000. He worked at the Nuclear Reactor Laboratory in Huarangal, Lima for two years. During that time he developed a graphic interface for the Peruvian Nuclear Reactor RP10 as part of his thesis work to obtain the Licence in Physics.

He worked as Physics lecturer at the Universidad Tecnologica del Peru in Lima during the years of 2003 to 2006. After that, he joined the Master of Physics Program at the University of Texas at El Paso in the spring of 2007 where he obtained his Masters in Physics during the summer of 2009 with his thesis entitled "Characterization of Aerosols in the El Paso-Juarez Airshed". After finished his Master, he was admitted to the Doctoral Program of Computational Sciences in the Fall of 2009 where in 2012 he published his research work about "Single Scattering Albedo Retrievals in the El Paso-Juarez Airshed" in the Atmospheric Environment Journal.

This work is product of his research in light scattering by aerosol particles and its application in visibility in the El Paso del Norte region and it is the baseline for his doctoral proposal.

Permanent Address: 3512 Hixson St

El Paso, TX 79902

This dissertation was typed by Richard Medina Calderon.